able fraction of the cases the primary particle was noticeably scattered) shows that most of the protons responsible for the observed events have energies between about $2 \cdot 10^9$ and $5 \cdot 10^9$ ev. In fact, only the few events of the fourth group in Table 1 (two or more penetrating secondaries) require primary energies appreciably greater than $5 \cdot 10^8$ ev/c.

Events of types b and d (or e) in Fig. 8.1.25 correspond presumably to collisions in which a proton loses only a small fraction of its energy during its traversal of a nucleus. Events of type a, c, and f are possible examples of "charge exchange" (see § 7.1), i.e., of collisions in which a proton changes into a neutron that carries a large fraction of the initial proton energy, leaving a comparatively small amount of energy in the target nucleus. Or they may represent cases in which the proton suffers several collisions in the nucleus and thus loses most of its energy.

As a final remark, we may mention that in only a very small fraction of the events recorded in this experiment was there evidence for the production of mesons or photons.

Figure 8.1.18e illustrates another simple triggering arrangement used by Gregory and Tinlot in some of their experiments. In this case the operation of the chamber was controlled by the signal from a cosmic-ray telescope placed below the chamber. A picture was taken whenever a pulse from the telescope was not accompanied by a pulse from a large tray of counters placed above the chamber. Lead absorbers of various thicknesses were present between the counters of the telescope. The arrangement thus favored the recording of nuclear events initiated by non-ionizing rays (i.e., by neutrons) and giving rise to penetrating particles.

Figure 8.1.26 shows examples of the pictures obtained. In Table 2 the observed events are classified according to the multiplicity of penetrating particles and electronic showers. If one compares the results of this experiment with those of the experiment described previously, one notices that high-energy interactions account now for a much larger fraction of the events recorded. This is easily explained by the requirement that at least one penetrating particle be present among the secondary products of the interactions. Indeed, this requirement sets a lower limit of about 400 Mev to the energy of the primary neutron.

The probability of detection, of course, is an increasing function of the multiplicity of the secondary penetrating particles and also depends on the presence of electronic showers. The triggering arrangement is sufficiently simple so that one can compute this detection probability approximately for the various kinds of events listed in Table 2. One can thus correct the observed rates and obtain an estimate for the true rates. The result of such a computation is shown in the table.

Most interactions of type 1 in Table 2 (Fig. 8.1.26a) probably represent phenomena of charge exchange, whereby neutrons change into protons, leaving only a small fraction of their energy in the nucleus where the

Table 8.9.2. Classification of the nuclear interactions observed with the experimental arrangement shown in Fig. 8.1.18e. [The 136 nuclear interactions were due to non-ionizing primaries and occurred in the first through tenth plates. n_{pp} represents the number of penetrating secondary particles; n_{sh} represents the number of secondary electronic showers. Classes 1 through 8 include events in which the total energy of electronic showers, E_{sh}, is less than 1 Bev. Class 9 includes events giving rise to electronic showers of energy greater than 1 Bev. In these events it is often difficult to identify penetrating particles. From Gregory and Tinlot (GBP51).]

Description of Event	Example of Event (Fig. 8.1.26)	Number of Interactions	Corrected Relative Frequency	Ratio of Interactions in Pb and Al
Group I:				
1. $n_{pp} = 1$, $n_{sh} = 0$.	a	36	0.61	
2. $n_{pp} = 1$, $n_{sh} \geq 1$, $E_{sh} < 1$ Bev.	b	5	0.08	2.3 ± 0.6
3. $n_{pp} = 2$, $n_{sh} = 0$.	c	20	0.16	
4. $n_{pp} = 2$, $n_{sh} \geq 1$, $E_{sh} < 1$ Bev.	—	7	0.06	
Group II:				
5. $5 \geq n_{pp} \geq 3$, $n_{sh} = 0$.	—	9	0.06	
6. $n_{pp} \geq 3$, $n_{sh} \geq 1$, $E_{sh} < 1$ Bev, $n_{pp} + n_{sh} \leq 6$.	d	25		5.0 ± 1.4
7. $n_{pp} \geq 7$, $n_{sh} = 0$.	—	2	0.01	
8. $n_{pp} \geq 3$, $n_{sh} \geq 1$, $E_{sh} < 1$ Bev, $n_{pp} + n_{sh} \geq 7$.	e	12		
9. $n_{pp} \geq 3$, $n_{sh} \geq 1$, $E_{sh} > 1$ Bev.	f	20	0.02	

interaction occurs. Since the energy spectrum of the primary neutrons is certainly a rapidly decreasing function of the energy, the majority of the neutrons giving rise to events of type 1 must have energies not much greater than the minimum required energy of about 400 Mev.

From the experiments described it is also possible to determine whether or not the simple phenomenon of charge exchange occurs frequently at energies considerably greater than about 400 Mev. Indeed, if neutrons of several Bev energy or more could turn into protons of nearly equal energy one should observe events of type 1 followed by high-energy interactions of the resulting proton. Gregory and Tinlot did not observe any such succession of events. From a detailed analysis of their data they concluded that during the course of their experiments, neutrons with more than about 4 Bev energy had traversed a total thickness of 1,000 g cm^{-2}

of lead and 600 g cm^{-2} of aluminum without undergoing a single process of charge exchange. Therefore this process appears to be unlikely at high energies.

The reader will find further statistical data on the types of nuclear interactions observed with the cloud-chamber technique and on the secondary particles arising from these interactions in the papers of Fretter (FWB48 and FWB49.1), of Chao (CCY49), and of Butler, Rosser, and Barker (BCC50).

8.10. ***The nature and the energy distribution of the secondary ionizing particles from nuclear interactions.*** The following four sections give a brief account of the experiments that have served to identify the secondary particles arising from nuclear interactions of cosmic rays and to estimate their energy spectrum.

Observations by various experimenters with Ilford C2 emulsions have supplied abundant information regarding the nature and the energy distribution of the comparatively slow disintegration products that give rise to dense tracks (these, of course, are the only tracks detected by electron-insensitive emulsions). It appears that close to 1/3 of the dense tracks are due to multiply charged particles and about 2/3 to singly charged particles (HJB49.3; PN50; PDH50; BHL50.2; AMM51). Of the multiply charged particles the majority [perhaps 80 to 90 per cent; see Bradt and Kaplon (BHL50.2)] are α-particles and the remainder heavier nuclei. Of the singly charged particles 80 to 90 per cent are protons (BHL50.2; HJB49.3) and the remainder deuterons and tritons. There is some indication that the ratio of singly to multiply charged particles depends somewhat on the class of stars considered (AMM49; PN50; PDH50), but the data of the various experimenters are not in agreement on this subject.

Since most of the stars seen in photographic emulsions originate from silver or bromine, the remarks in the preceding paragraph refer mainly to the properties of stars arising from the disintegrations of heavy nuclei. Experiments with sandwich emulsions indicate that multiply charged particles (mainly α-particles) account for about 50 per cent of the tracks in stars originating from light elements (PDH50).

The histograms in Fig. 1 summarize the results obtained by Harding, Lattimore, and Perkins (HJB49.3) and by Perkins (PDH50) on the energy distribution of protons and α-particles in groups of stars with different total numbers of dense prongs. The energies of the protons were determined by grain-counting, the energies of the α-particles by their range in the emulsion. The α-particle distributions were then corrected to account for the α-particles escaping from the emulsion before reaching the end of their range.

It is reasonable to assume that all stars with 7 or more dense prongs belong to nuclei of silver or bromine. Conceivably, the disintegration of an oxygen nucleus could give rise to an 8-prong star. However, the probability of this event is small because, as already noted, the nucleus does not usually break up into individual protons and neutrons. Stars with less than 7 prongs may originate from light or heavy nuclei. In the preparation of the graphs concerning stars with small numbers of prongs the estimated contribution from the light nuclei has been subtracted, so that the results presented in Fig. 1 refer to heavy nuclei alone.

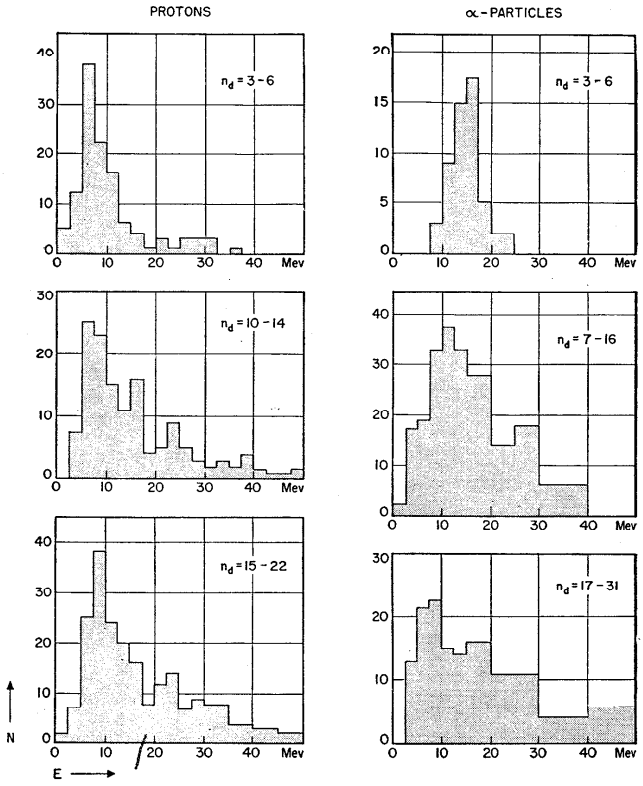

Fig. 8.10.1. Energy distribution of protons and α-particles emitted from silver and bromine nuclei in stars with different total numbers, n_d, of dense prongs. Observations with Ilford C2 emulsions. [From Perkins (PDH50).]

Figure 1 shows that the energy distribution of protons and α-particles changes with the number of particles per star. In the case of protons, the average energy per particle increases with the number of particles. In the case of α-particles there is no clear change in the average energy per particle, but the energy distribution becomes broader as the number of particles per star increases.

Work by the Bristol group with electron-sensitive emulsions has provided information concerning the nature and the energy distribution of the lightly ionizing products of nuclear interactions [see § 8.8 and refs. (FPH50), (CU50)].

Figure 2 summarizes the results of measurements made on tracks longer than 3 mm appearing on plates exposed at an average altitude of 21,000 meters. In this figure, the ordinate represents the grain density, which is a function of the particle velocity, β, and the abscissa represents the mean angle of scattering, which is a function of the product, βp, of the velocity and the momentum (see §§ 3.15 and 3.16). The curves show the computed relation between grain density and mean scattering angle for different kinds of particles, i.e., μ-mesons, π-mesons, protons, deuterons, tritons, and α-particles. The dots represent experimental determinations. The open dots correspond to secondary particles, the solid dots to primary particles.

We have noted previously that α-particles account for a considerable fraction of the comparatively slow particles producing dense tracks. Figure 2 shows, instead, that practically all of the secondary particles of higher energy are singly charged. This means that secondary α-particles of relativistic velocities are very rare. (However, Fig. 2 shows also that at balloon altitudes α-particles of relativistic velocities are fairly common among the initiating particles; see § 8.22 below.)

For sufficiently small energies, i.e., for sufficiently large values of the mean scattering angle, the method affords an unambiguous separation between mesons and heavier particles (protons, deuterons, tritons). The accuracy seems to be adequate also to establish the fact that all or almost all of the mesons created with kinetic energies less than about 150 Mev are π-mesons. If μ-mesons are present, their number is less than 2 per cent of the number of π-mesons, according to an estimate of Fowler (FPH50). There is no indication for the existence of high-energy electrons among the secondary particles of nuclear interactions. Protons, deuterons, and tritons are not sharply separated. There is, however, a clear indication that the heavier hydrogen isotopes, even though less abundant than protons, are present in substantial numbers.

The distinction between mesons and heavier singly charged particles becomes more and more difficult as the energy increases and is practically impossible for energies greater than about 1 Bev. Up to this energy, the number of protons, deuterons, and tritons is greater than the number of

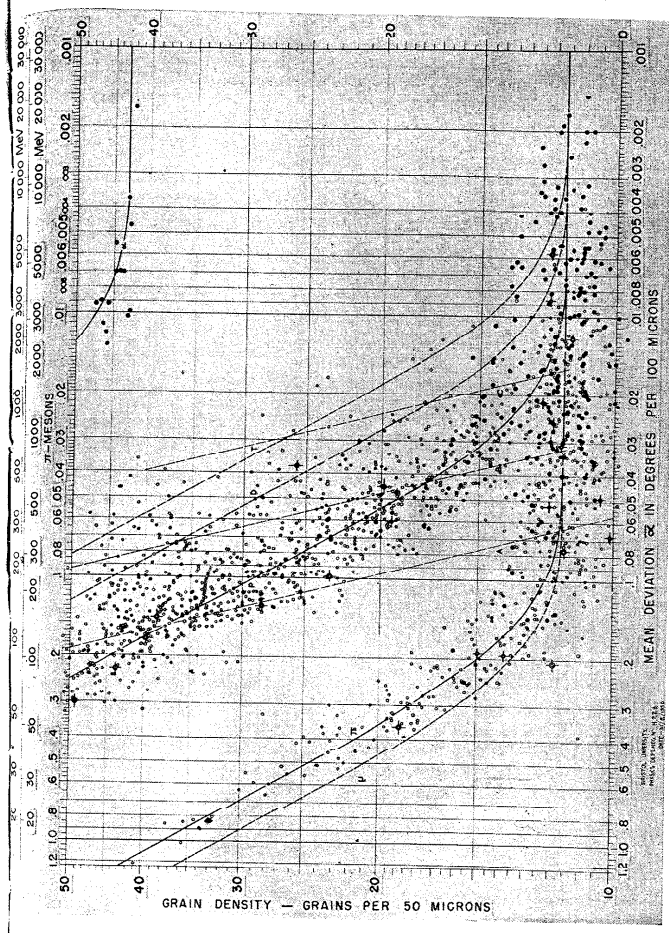

Fig. 8.10.2. Relation between grain density and scattering angle for the tracks of 700 particles recorded at 50 g cm^{-2} atmospheric depth in Ilford G5 electron-sensitive emulsions. The lines marked μ, π, P, D, T, and α represent the computed relations between grain density and scattering angle for μ-mesons, π-mesons, protons, deuterons, tritons, and α-particles. A, B, and C are lines of constant momentum and correspond respectively to 500, 1000, and 2000 Mev/c. [From Cannerini and his collaborators (CU50).]

π-mesons; the ratio between the two numbers, however, seems to decrease with increasing energy. Because of their smaller mass, mesons of a given energy have a much greater velocity, and thus produce tracks with a much smaller grain density than protons or heavier particles of the same energy. Therefore most of the mesons give rise to thin tracks, whereas most of the protons, deuterons, and tritons give rise to medium or dense tracks.

Figure 3 shows the differential energy distributions of mesons, protons, deuterons, and tritons, as obtained from the experimental data summarized in Fig. 2. As pointed out above, mesons with energy less than

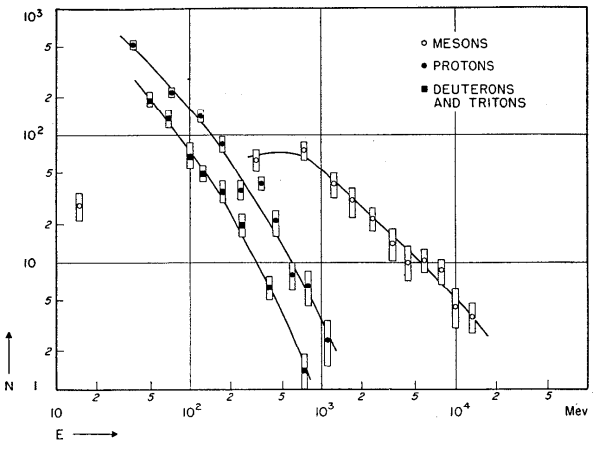

Fig. 8.10.2. Differential distribution in kinetic energy for the various types of particles at 50 g cm^{-2}. The point at 1.6 Mev for mesons, is for π^--particles only and is calculated from the observed number of mesons which are ejected from stars and produce nuclear disintegrations at the end of their range. To obtain the number of particles per star per Mev interval multiply by $\sim 2.5 \times 10^{-5}$. [From Camerini *et al.* (CU50).]

150 Mev can be directly recognized as π-mesons. Above 150 Mev, an experimental separation between π- and μ-mesons is no longer possible. However, it seems natural to assume that in the high-energy region as well, all, or almost all, of the mesons belong to the π-variety.

If (more or less arbitrarily) one extrapolates the spectra shown in Fig. 3 with curves obeying an $E^{-2.5}$ law (see § 8.14) one obtains the values summarized in Table 1 for the relative numbers of mesons, protons, deuterons, and tritons responsible for tracks of different categories.

Table 8.10.1. Percentage of different kinds of particles responsible for the singly charged secondaries from stars. [(The grain density of medium tracks is here between 1.5 g_{min} and 4 g_{min}). From the data of Camerini *et al.* (CU50).]

	Classification by Grain Density		Classification by Kinetic Energy E (Mev)		
	Medium	Thin	$50 < E < 100$	$E > 100$	$E > 1000$
π-mesons	36	79	15	32	71
Protons	51	17	56	50	26
Deuterons and Tritons	13	4	29	18	3

The cloud-chamber method is less effective than the method of the photographic emulsion in separating mesons from the heavier singly charged particles among the secondary products of nuclear interactions. Among the results of cloud-chamber experiments that bear upon this question we wish to mention here those of Butler, Rosser, and Barker (BCC50). These experimenters used a magnet chamber and were thus able to determine the sign of the charge for a number of secondary penetrating particles. In a group of 67 measurable tracks they found 52 positive and 15 negative particles. The negative particles must be interpreted as mesons. If one assumes that the number of positive mesons roughly equals that of negative mesons, one concludes that about half of the penetrating particles are protons and half mesons. In this experiment the maximum detectable momentum was $8 \cdot 10^9$ ev/c and conditions were such that a π-meson had to have a momentum greater than $2.3 \cdot 10^8$ ev/c and a proton a momentum greater than $5.7 \cdot 10^8$ ev/c to be recognized as a penetrating particle. These results are not in disagreement with those for the proportion of protons and mesons from stars, found by the method of the photographic emulsion.

As pointed out in § 8.6, it is reasonable to assume that the disintegration of a heavy nucleus following the collision of a high-energy particle proceeds in two separate steps. The first is the ejection from the nucleus of mesons and of high-energy nucleons; the second is the "evaporation" of the residual highly excited nucleus. The dense tracks of stars observed in photographic emulsions are produced to a large extent by particles emitted during the evaporation process. The number of these particles is a function of the excitation energy.

Several authors have attempted to explain the energy distributions of the low-energy protons and α-particles from stars (see Fig. 1) on the basis of the evaporation model (BgH44; HzW49; HJB49.3; LCK50). It is still uncertain how closely this model will be able to account for the experimental data, especially because it is not yet clear how many of the low-

energy particles from stars are emitted during the initial stage of the interaction rather than during the subsequent evaporation process.

Since most of the thin tracks are due to mesons, and most of the dense and medium tracks are due to protons and heavier nuclear fragments, one may estimate crudely the total energy expended in the production of secondary nucleons and heavier fragments by summing the energies of all dense and medium tracks, adding the estimated energies of the undetectable neutrons that must be produced simultaneously with the protons, and adding also the binding energies of the emitted particles. In this manner Brown and her collaborators (BRH49.1) obtained the results shown in Fig. 4. The curve drawn through the experimental points obeys the empirical relation:

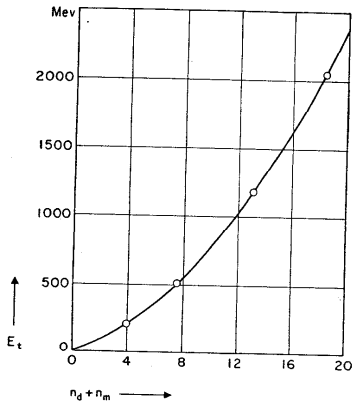

Fig. 8.10.4. Average energy release, E_t, in stars with different numbers of dense plus medium tracks, $n_d + n_m$. The energy plotted as ordinate includes only the energy associated with particles having more than 1.5 times minimum ionization, corrected for the energy carried by the undetectable neutrons (total neutron energy taken as 1.25 times the proton energy). [From Brown, *et al.* (BRH49.1).]

$$E_t = 37(n_d + n_m) + 4(n_d + n_m)^2$$

where E_t is the total energy in Mev as defined above and $n_d + n_m$ is the total number of dense and medium tracks. This relation shows that the average energy per particle increases linearly with the number of particles.

Different classes of stars are certainly correlated to different energy groups of the initiating particles as shown, for example, by the different

results obtained at different altitudes on the distribution of stars according to the number of prongs (see § 8.8).

This correlation, of course, must not be understood as a one-to-one correspondence, because the events occurring when a high-energy particle passes through a nucleus are of a statistical nature. On the average, however, one may predict that both the number of mesons and the number of high-energy nucleons resulting from a nuclear interaction are increasing functions of the energy of the initiating particle. In fact, as the energy of the initiating particle increases, the average energy of the secondary particles (nucleons and π-mesons) arising from the primary's first collision in the nucleus increases too. Therefore a greater proportion of these secondary particles becomes capable of producing tertiary high-energy nucleons and mesons by further collisions within the nucleus. Moreover, if multiple production of mesons occurs, the multiplicity is probably an increasing function of the primary energy.

Each fast particle produced in the nucleus has a certain probability of losing a fraction of its energy before escaping from the nucleus. Therefore one may predict that the average excitation energy of the residual nucleus, and therefore the number of low-energy disintegration products, are increasing functions of the number of fast particles emitted during the initial stage of the interaction. The experimental results seem to confirm this prediction. One finds, for example, that on the average the number of medium tracks, n_m, and the number of dense tracks, n_d, per star increase with each other. This is shown by Fig. 5, obtained from the data of Brown and her collaborators already quoted, in which n_d is plotted against n_m.* Also, Tables 8.8.1 and 8.8.2 show that, on the average, the number of thin tracks (characteristic of mesons) is an increasing function of the number of medium and dense tracks (characteristic of protons and heavier nuclear fragments).

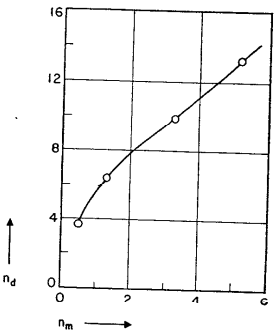

Fig. 8.10.5. Average number per star of dense tracks, n_d, as a function of the number of medium tracks, n_m. [From the observations of Brown, *et al.*, (BRH49.1) at 3,460 meters.]

* The reader may recall the opposite result of an experiment performed with artificially accelerated protons (§ 7.9). In this experiment the star-producing radiation was mono-energetic. Therefore there was a constant amount of energy available, which could be split in different proportions between secondaries of different energies.

8.11. ***The production of photons in nuclear interactions.*** The early cloud-chamber pictures of nuclear interactions had shown the existence of secondary particles capable of initiating electronic showers, but had failed to determine whether these particles were electrons or photons. The electronic showers appeared to originate from the same plate where the nuclear interaction had occurred, indicating that the multiplication process had begun before the initiating particles escaped from the plate. Since the plates were made of lead and were several radiation lengths in thickness, this was to be expected regardless of whether the initiating particles were electrons or photons.

More recently Gregory, Rossi, and Tinlot (GBP50) have succeeded in detecting the production of photons in nuclear interactions of cosmic rays by using a cloud chamber containing alternate plates of aluminum and lead. Figure 8.1.18e shows the actual experimental arrangement. The probability of pair production by a high-energy photon traversing one of the aluminum plates (0.79 cm thick) was only 7 per cent. Therefore it was anticipated that practically all of the photons produced in the aluminum plates would emerge from these plates without interacting and would initiate showers in one of the following lead plates.

Gregory and his collaborators obtained a number of pictures showing the expected "non-ionizing link." A particularly clear example is reproduced in Fig. 8.1.32. Other examples are shown in Figs. 8.1.28 and 8.1.31. Figure 8.1.29 shows a beautiful example of photon production obtained by Barker (BRP51) with a cloud chamber containing plates of carbon and lead.

Work with photographic emulsions has also provided evidence for the production of photons in nuclear interactions of cosmic rays [see ref. (KMF49) and § 8.22] even though, as pointed out in § 8.1, the photographic emulsion is a less effective detector of photons than the multiple-plate cloud chamber.

In an attempt to determine whether or not *all* of the shower-initiating particles arising from nuclear interactions are photons, Gregory and Tinlot investigated the point of origin of 80 electronic showers appearing in a series of pictures of nuclear interactions. The result of this analysis is shown in Table 1. In a number of cases the presence of other tracks obscured the origin of the shower. These cases are listed in the last two columns, under headings indicating the plates in which the shower might have originated.

Table 1 lists the computed values of the probability that a photon produced at a random depth in a given plate (plate #1) undergoes materialization in the plate of production or in the various other plates. If all showers are produced by photons, their points of origin should be distributed among the various plates in proportion to this probability, with no ionizing link between the point of origin of the nuclear interaction and the point of origin of the shower, when the two points are in different plates. Within the large statistical errors, the experimental results agree with this conclusion. Particularly worthy of notice is the fact that none of the pictures of nuclear interactions occurring in one of the aluminum plates shows either a shower or a shower-producing ionizing particle starting from the plate where the interaction occurs.

Table 8.11.1. Starting point of showers produced in nuclear interactions. [Plate #1 is the plate in which the nuclear interaction occurred; plate #2 the one immediately below, and so on. From Gregory and Tinlot (GBP51).]

Interactions in Lead

	Plate #1	Plate #2	Plate #3	Plate #4	Plate #5	Other Plates	Plate #1, 2, or 3	Plate #3, 4, or 5
Beginning of shower:	Pb	Al	Pb	Al	Pb			
Observed number of showers:	19	1	10	0	4	0	15	3
Calculated probability for materialization of a photon:	35%	4%	36%	1%	14%	10%	—	—

Interactions in Aluminum

	Plate #1	Plate #2	Plate #3	Plate #4	Plate #5	Other Plates (below #5)	Plate #1 or 2	Plate #2, 3, or 4
Beginning of shower:	Al	Pb	Al	Pb	Al			
Observed number of showers:	0	13	0	5	0	0	6	4
Calculated probability for materialization of a photon:	3%	58%	2%	21%	1%	15%	—	—

The above results, together with the fact that none of the tracks from stars observed in photographic emulsions were identified as those of high-energy electrons (see § 8.10), strongly support the view that all of the showers associated with nuclear interactions originate from photons.

As already pointed out, it is natural to assume that some, and possibly all, of these photons arise from the decay of short-lived neutral mesons.* Since each neutral meson disintegrates into two photons, one should often

* There is, however, the possibility that some photons (mostly of not very high energy) may arise from processes of charge acceleration connected with the nuclear interactions, in particular with the production of charged mesons (SLI49.3).

observe showers with double cores. [Of course showers with single cores will not be uncommon because one of the two photons may escape from the chamber without interacting or may not have enough energy to produce a clearly recognizable shower. Note, in this connection, that the energy of a photon emitted in the direction opposite to that of the neutral meson tends to zero as the meson energy increases and is only 5 Mev for a meson energy of 10^9 ev; see Eq. (4.13.8).]

The principles of conservation of energy and momentum yield a simple relation [see Eq. (4.15.5)] between the energies, E_1, E_2, of the two photons arising from the decay of a neutral meson in flight and the angle, θ, enclosed by their trajectories. If this angle is sufficiently small so that sin $(\theta/2)$ may be taken as equal to $\theta/2$, this relation becomes:

$$\theta = \frac{m_0 c^2}{\sqrt{E_1 E_2}} \tag{1}$$

where m_0 is the mass of the neutral meson.

Many pictures of double-core showers are available. Sometimes one can measure the angle between the cores with fair accuracy, and one can also obtain a crude estimate of the energies of the two photons from the size of the showers. One can then check Eq. (1) and thereby test the assumption that the two photons arise from the decay of one neutral meson. Examples of such an analysis will be found in the captions of Figs. 8.1.24, 8.1.28, and 8.1.29.

Often Eq. (1) appears to be satisfied within the errors of the measurements, but sometimes the experimental values of θ, E_1, and E_2 seem to contradict this theoretical relation. Of course, one can never be absolutely sure that any pair of photons appearing in the cloud chamber is actually the decay product of a single neutral meson. Because of this circumstance and because of the large uncertainty in the evaluation of the photon energies and of the angle between their trajectories, one can only conclude that present experimental data are not in obvious disagreement with the assumption that the decay of neutral mesons is the source of all photons associated with nuclear interactions of cosmic rays.

It is interesting to note that, under this assumption, the number of the neutral mesons is of the same order as that of the penetrating particles. For example, Gregory and Tinlot in 82 pictures of nuclear events obtained with the experimental arrangement shown in Fig. 8.1.18e observed 355 penetrating particles and 148 electronic showers. If one assumes that the photons responsible for the showers are due to the decay of neutral mesons, and if one makes a crude estimate of the number of photons that might have escaped detection, one finds a value of about 110 for the number of neutral mesons. Since some of the penetrating particles are protons, one concludes that the average number of neutral mesons produced in high-energy nuclear interactions is perhaps somewhat smaller, but in any case of the same order

of magnitude as the number of charged mesons. A similar conclusion was reached by Fretter (FWR49.1) on the basis of his experimental results.

It is also interesting to recall the results, presented in Table 8.9.2, concerning the frequency of occurrence of electronic showers in nuclear events of different kinds. One sees from this table that the fractional number of nuclear events accompanied by electronic showers increases rapidly with the multiplicity of the secondary penetrating particles. A likely interpretation of this result is that the events of small multiplicity are due to primary particles of comparatively low energy for which the production of mesons (charged or neutral) is an unlikely phenomenon. For example, most of the events of type 1 in Table 8.9.2 are probably cases of charge exchange with no meson production, as already noted. When interpreting the experimental results, one should also remember that neutral mesons with energies of the order of 10^8 ev or less do not give rise to conspicuous showers and are therefore more difficult to detect than charged mesons of the same energy, whereas for energies of the order of several Bev or more the situation is reversed.

8.12. ***The identification of π-mesons in penetrating showers.*** Piccioni (PO50) performed an ingenious experiment which clearly demonstrates the presence of π-mesons among the secondary products of high-energy nuclear interactions. He used for this experiment the apparatus shown schematically in Fig. 1, where the circles represent Geiger-Mueller tubes and the black areas, lead. The space marked "abs" was filled either with carbon or with sulphur. The equipment was operated at an altitude of 3,400 meters.

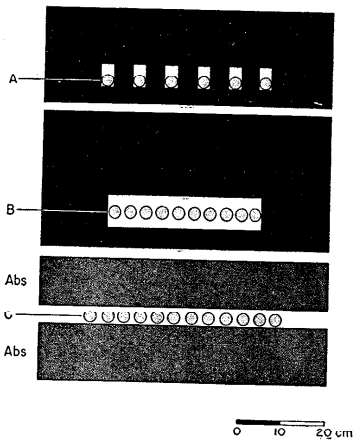

Fig. 8.12.1. Apparatus used by Piccioni to study the production of charged π-mesons in local penetrating showers. [From Piccioni (PO50).]

Electronic circuits recorded the following events: coincidences ABC, delayed coincidences $(A_1B[C]_d)$, coincidences $(A_{\geq 2}B)$ and delayed coincidences $(A_{\geq 2}B[C]_d)$.

The symbol (ABC) indicates, as usual, an event causing simultaneous discharges of at least one tube in each of the three trays A, B, and C. Most events of this kind correspond to the passage of μ-mesons through the instrument.

The symbol $(A_1B[C]_d)$ represents an (AB) coincidence involving the discharge of *only one* tube in tray A and followed, with a delay between 1.3 and 8.5 microseconds, by a discharge in one of the counters in tray C. An event of this kind usually indicates the arrival from the atmosphere of a μ-meson that traverses trays A and B, comes to rest in the absorber either above or below tray C, and subsequently decays giving rise to an electron that discharges tray C. Note that if one of counters C is discharged simultaneously with tray A and B (for example by a meson stopping in the absorber *below* tray C), this counter remains inactive for more than 100 microseconds (see § 3.6). The other counters of tray C, however, do not become insensitive and are therefore still capable of recording a delayed coincidence.

The symbol $(A_{\geq 2}B)$ indicates an event causing simultaneous discharges in *two or more* of the A tubes and in one or more of the B tubes. Events of this kind are due primarily to local penetrating showers (see § 8.2) originating for the most part in the lead above tray A.

Electronic showers initiated by electromagnetic interactions of μ-mesons can also produce $(A_{\geq 2}B)$ coincidences. However, the presence of 3.8 cm of lead between the tubes of tray A greatly decreases the number of coincidences arising from events of this kind. Piccioni made an estimate of the actual fraction of $(A_{\geq 2}B)$ coincidences due to penetrating showers, with the following argument. The rate of occurrence of high-energy nuclear interactions increases by a factor of about 18 from sea level to 3,400 meters (see Fig. 8.4.3). According to Piccioni's own measurements, the corresponding increase factor was 8.6 for events $(A_{\geq 2}B)$ and 1.95 for events (ABC). Assume that the rate of $(A_{\geq 2}B)$ coincidences due to secondary effects of μ-mesons is proportional to the rate of (ABC) coincidences; call x the relative number of $(A_{\geq 2}B)$ coincidences at 3,400 meters due to secondary effects of mesons; then $1 - x$ is the relative number of coincidences due to nuclear interactions. One obtains for x the equation:

$$\frac{(1-x)}{18} + \frac{x}{1.95} = \frac{1}{8.6},$$

from which it follows $x = 0.13$. Thus 87 per cent of the $(A_{\geq 2}B)$ coincidences recorded at 3400 m are due to nuclear interactions (at sea level, however, only about 40 per cent of such coincidences would be due to nuclear interactions).

The symbol $(A_{>2}B[C]_d)$ indicates an $(A_{\geq 2}B)$ coincidence followed by a delayed discharge in one of counters C. Presumably, events of this kind are due to penetrating showers giving rise to mesons, which stop in the absorber and subsequently decay.

The experimental results are summarized in Table 1. One sees that delayed coincidences $(A_{\geq 2}B[C]_d)$ do occur and that their number is of the order of one per cent of the number of $(A_{\geq 2}B)$ coincidences. Since only a small fraction of the mesons stop in the absorber and since not all of the decay electrons originating in the absorber are detected, one concludes that mesons must be abundantly represented among the secondary particles in the penetrating showers responsible for the $(A_{\geq 2}B)$ coincidences. By subdividing the delayed coincidences into four channels,

Table 8.12.1. Summary of data taken by Piccioni (PO50) with the experimental arrangement shown in Fig. 8.12.1, at an altitude of 3,400 meters. The total time of observation was about 200 hours with each absorber. [The delayed coincidence counting rates are corrected for accidental coincidences.]

Absorber	ABC (counts/hr)	$A_1B[C]_d$ (counts/hr)	$A_{\geq 2}B$ (counts/hr)	$A_{\geq 2}B[C]_d$ (counts/hr)
Graphite	5730 ± 5	30.4 ± 0.5	98.6 ± 0.7	1.17 ± 0.07
Sulphur	5680 ± 5	16.4 ± 0.4	102 ± 0.7	1.06 ± 0.07

Piccioni was able to verify the exponential distribution in time of the decays, and found that the decay curves corresponding to events $(A_1B[C]_d)$ and $(A_{\geq 2}B[C]_d)$ were consistent with the known mean life of μ-mesons.

Delayed coincidences, of course, will occur whether the mesons stopping in the absorber are π-mesons or μ-mesons. In fact, positive π-mesons, after coming to rest, decay with a mean life of approximately $2.65 \cdot 10^{-8}$ sec into μ-mesons of 4 Mev energy. These, in turn, stop after traveling a distance of the order of a millimeter and then decay with their proper mean life of $2.1 \cdot 10^{-6}$ sec. Because of the very short mean life of π-mesons, the time distribution of delayed pulses arising from the double $\pi \rightarrow \mu \rightarrow e$ decay process does not differ appreciably from the exponential distribution corresponding to a simple $\mu \rightarrow e$ decay.

However, a comparison between the results obtained with carbon and sulphur absorbers offers a clue to the identity of the mesons.

Assume first that the mesons stopping in the absorber are μ-mesons. Positive μ-mesons undergo spontaneous decay both in carbon and in sulphur. In carbon, practically all negative μ-mesons, too, undergo spontaneous decay. In sulphur, however, 72 per cent of the negative μ-mesons undergo nuclear absorption and only 28 per cent of them undergo spontaneous decay. Moreover, the competition between spontaneous decay and nuclear absorption reduces their mean life to about 0.54 microseconds (see Table 4.9.1). Therefore only a negligible fraction of the negative μ-mesons stopping in sulphur will decay after a time longer than 1.3 microseconds, the minimum delay required in order that a delayed coincidence may be recorded.

Since the carbon and sulphur absorbers used in Piccioni's experiment have approximately the same stopping power, it follows from the above arguments that changing the absorber from sulphur to carbon must increase the number of delayed coincidences due to μ-mesons in the ratio of the number of positive particles to the total number of positive and negative particles. This conclusion is borne out by the observations on $(A_1B[C]_d)$ events, which are due, as already pointed out, to the stopping of μ-mesons from the atmosphere. The observed carbon to sulphur ratio of 1.85 ± 0.05

(see Table 1) is consistent with the assumption that the ratio of positive to negative μ-mesons in the atmosphere is about 1.15, a figure in agreement with other experimental data.

Assume next that the mesons stopping in the absorber are π-mesons. In this case negative mesons undergo nuclear absorption in carbon as well as in sulphur, whereas positive mesons undergo spontaneous decay in both substances. Therefore the rate of delayed coincidences observed with the two absorbers must be the same. Table 1 shows that the counting rates for the events $(A_{\geq 2}B[C]_d)$ recorded with carbon and sulphur are actually equal within the statistical error of 10 per cent. One thus concludes that most, and possibly all, mesons arising in penetrating showers, unlike those present in the atmosphere, are π-mesons.* This result confirms the results of observations with photographic emulsions discussed in § 8.10.

Conversi and Ticho (CM50) have described an experimental arrangement for the separation of π- from μ-mesons, based upon the same principle as that of Piccioni.

The production of mesons in penetrating showers has also been detected by Walker with a similar experimental method (WWD50.1).

8.13. ***Production of low-energy neutrons in nuclear interactions.*** The experiments described in the preceding sections do not furnish any information on the emission of neutrons whose energy is smaller than the minimum energy necessary for the production of secondary nuclear stars; i.e., smaller than about 50 Mev. On general grounds, there are reasons to believe that such neutrons should be represented abundantly among the secondary products of high-energy nuclear interactions. In fact, one should expect to find approximately equal numbers of neutrons and protons among the nucleons knocked out from the nucleus directly, whereas neutrons should be more numerous than protons among the nucleons of lower energy resulting from the evaporation of the highly excited nucleus. This is especially true in the case of heavy nuclei, where the electric field surrounding the nucleus inhibits the emission of low-energy protons.

Cocconi and his collaborators (CG48; CG49.2; CG50) and Montgomery and Tobey (MCG49.1) succeeded in demonstrating experimentally the production of neutrons of several Mev energy in the nuclear interactions of cosmic rays by first slowing down these neutrons with paraffin and then detecting them by means of boron trifluoride counters (see § 3.4). For practical purposes, one may assume that these counters respond only to thermal or epithermal neutrons, as the cross-section for the $B^{10}(n,\alpha)Li^7$ reaction is inversely proportional to the neutron velocity.

Figure 1 shows the experimental arrangement used by Cocconi and his

* Strictly speaking, of course, the experiment described does not rule out the production of other strongly interacting particles (e.g., V-particles) capable of disintegrating into π- or μ-mesons.

collaborators in one of their experiments (see CG50) at 3,260 m altitude. a, b, and c are trays of Geiger-Mueller tubes; A, B, C, and D are trays of enriched boron trifluoride counters embedded in a large block of paraffin. Blocks of different materials can be placed in the position marked Σ.

Each coincidence between trays b and c initiates a 10-microsecond square pulse with a 5-microsecond delay. Whenever a coincidence occurs between this square pulse and at least one of the twenty neutron counters, a "master pulse" is generated. The master pulse activates a hodoscope of neon bulbs connected to the individual counters of trays a, b, and c, and to three additional counters s, not shown in the diagram. These counters are placed some distance away from the main part of the instrument, to discriminate against air showers. Each neon bulb of the hodoscope gives a flash whenever the corresponding counter is discharged within a 30-microsecond interval before the occurrence of the master pulse. The master pulse also starts a 330-microsecond sweep on a cathode-ray oscilloscope. The pulses of the neutron counters are brought to the vertical deflecting plates of this oscilloscope. Therefore the oscilloscope records all neutron pulses occurring during a 330-microsecond interval after the beginning of each master pulse. A camera, triggered by the master pulse, takes pictures of the neon bulbs and of the oscilloscope screen.

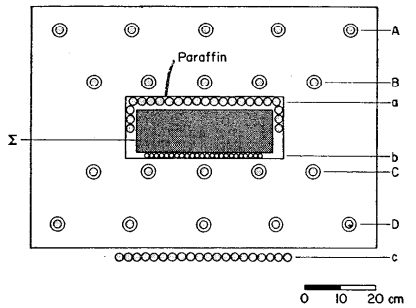

Fig. 8.13.1. Experimental arrangement used by Cocconi and his collaborators (CG50) to study the production of neutrons in nuclear interactions of cosmic rays.

The arrangement described above is designed to detect nuclear interactions produced in Σ by cosmic rays and giving rise to neutrons as well as to secondary ionizing particles. In order to be detected the neutrons must have fairly small energies (approximately between 1 and 15 Mev, according to an estimate of the authors), because neutrons of higher energies cannot be slowed down to thermal velocities by the paraffin block. The ionizing particles, on the other hand, must have a range of at least 22 g cm^{-2} of

paraffin and therefore a minimum kinetic energy of approximately 170 Mev if they are protons, or approximately 75 Mev if they are mesons.

As already explained in the discussion of a similar experiment (see § 4.12), the long mean life of thermal neutrons in paraffin requires that the neutron detector remain active for several hundred microseconds (330 in the present experiment) after the process in which the neutrons originate. On the other hand, it also allows one to initiate the sensitive period with some delay (5 microseconds in the present experiment), thereby eliminating various sources of spurious coincidences.

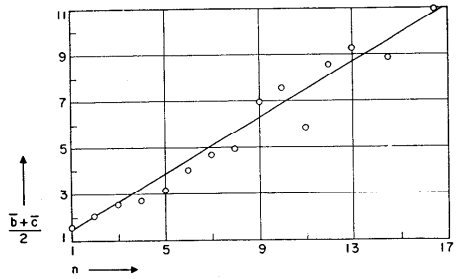

Fig. 8.13.2. The average number of b and c counters discharged, $(\bar{b} + \bar{c})/2$, versus the number, n, of neutrons recorded. Σ = 11.4 cm of Pb. [From Cocconi *et al.* (CG50).]

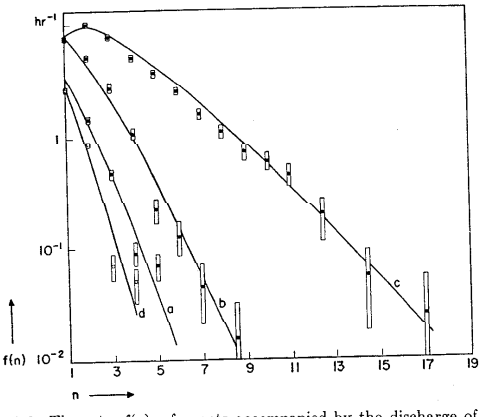

Fig. 8.13.3. The rate, $f(n)$, of events accompanied by the discharge of n neutron counters. Experimental arrangement shown in Fig. 8.13.1. (a) Σ = 0.63 cm Pb; (b) Σ = 2.54 cm Pb; (c) Σ = 11.4 cm Pb; (d) Σ = 12.0 cm Al. [From Cocconi *et al.* (CG50).]

Figures 2 and 3 show some of the experimental results obtained. Figure 2 gives the average numbers of Geiger-Mueller counters in trays b and c that were discharged simultaneously with different numbers of neutron counters. In this experiment the producing material in Σ was an 11.4-cm lead block. One sees that the multiplicity of neutrons per event increases with the multiplicity of ionizing particles. Up to 17 neutron counters were discharged in individual events. If one considers the efficiency of the neutron counters (about 0.03 according to the authors), one concludes that an individual event is occasionally capable of producing several hundred neutrons. Obviously such an event cannot correspond to the disintegration of a single lead nucleus, but must be the result of a chain of nuclear interactions.

Table 8.13.1. Summary of results derived by Cocconi *et al.*, from experimental data obtained with the arrangement shown in Fig. 8.13.1.

Material in Σ	Average Neutron Multiplicity
11.4 cm Pb	50
2.54 cm Pb	17
0.63 cm Pb	10
12.0 cm Al	6

Figure 3 shows the dependence of the counting rate on the number of neutron counters discharged, as measured with different producing layers in Σ. All counting rates are corrected for the background rate recorded with no producing layer in Σ. Table 1 lists the average multiplicities of neutrons in the events observed with 11.4, 2.54, and 0.63 cm of lead, and with 12 cm of aluminum. These numbers were computed from the experimental results and from the approximately known efficiency of the neutron detectors; their absolute values are uncertain by a factor of approximately two. From both Fig. 3 and Table 1, one can see that the rate of occurrence of events in which large numbers of neutron counters are discharged increases rapidly with increasing lead thickness.

All of the experimental results presented above clearly point to the existence of chains of nuclear interactions. High-energy nucleons and, probably, π-mesons arising from nuclear events produce further nuclear events and are responsible for the propagation of the chains. For not too large thicknesses of the producing layer, the average length of the chains, i.e., the number of successive nuclear interactions, must be an increasing function of this thickness. This explains the increase of the multiplicity of neutrons with thickness. A more detailed analysis shows that the experimental data can be interpreted quantitatively under the assumption that the interaction with each individual lead nucleus produces

on the average about 10 neutrons, and that the corresponding multiplicity for the interactions with aluminum nuclei is approximately 2 or 3. These numbers appear reasonable when compared with the average multiplicity of proton tracks in cosmic-ray stars observed with photographic emulsions, especially if one considers that neutrons must be more numerous than protons among the evaporation products of heavy nuclei.

To conclude the account of Cocconi's experiment, we may mention that, if one analyzes the data for discharges of tray a, one finds that the neutron-producing interactions originate from ionizing and non-ionizing primaries, in approximately equal numbers.

8.14. ***The energy spectrum of protons and neutrons in the atmosphere.*** In order to interpret nuclear interactions of cosmic rays, one often needs to know the energy spectrum of the particles responsible for such interactions. Unfortunately the experimental data relative to this question are very scarce and the conclusions that one may derive from these data are of a crude and tentative character.

All of the neutrons and practically all of the protons observed at moderate altitudes are secondary particles generated in nuclear interactions occurring in the atmosphere at some altitude above the place of observation. Therefore, the energy spectrum of these neutrons (or protons) is related to the energy spectrum of the neutrons (or protons) produced in nuclear interactions.

Let $s^{(n)}(E,x)$ represent the differential production spectrum of neutrons in the vertical direction at the depth x, so that $s^{(n)}(E,x)\,dE\,dx$ is the number of neutrons of energy between E and $E+dE$ produced in the air layer dx at the depth x, per cm²-second-steradian. Let $j^{(n)}(E,x)$ be the differential intensity in the vertical direction of neutrons present at the depth x, so that $j^{(n)}(E,x)\,dE$ equals the number per steradian of neutrons with energy between E and $E+dE$ incident upon 1 cm² in one second. Neutrons can be absorbed only by nuclear collisions; let L_c be the corresponding collision mean free path in the atmosphere. Between $j^{(n)}(E,x)$ and $s^{(n)}(E,x)$ there exists the relation:

$$j^{(n)}(E,x) = \int_0^x s^{(n)}(E,x')e^{-(x-x')/L_c}\,dx'. \tag{1}$$

The absolute number of neutrons produced in a layer of air of given thickness increases with decreasing x, but the shape of the energy spectrum probably does not change rapidly. If we neglect this change, and assume that L_c is independent of E, we may write the function $s^{(n)}(E,x)$ as the product of a function of E times a function of x. We then see from Eq. (1) that $j^{(n)}(E,x)$ and $s^{(n)}(E,x)$ have the same energy dependence.

A similar result holds for protons, as long as their energy is sufficiently large to justify the neglect of ionization loss. At lower energies, however, the ionization loss changes the shape of the observed spectrum considerably. In order to discuss this question quantitatively, let $j^{(n)}(E,x)$ represent the differential intensity and let $s^{(p)}(E,x)$ represent the production spectrum of protons. Consider (see Fig. 1) that a proton produced at the depth x' has a probability $\exp[-(x-x')/L_c]$ to arrive at the depth x without undergoing a nuclear encounter (if L_c is independent of energy), and that the protons arriving at the depth x with a residual range in dR at R are those produced at the depth x' with a residual range in dR at $R+x-x'$. Consider furthermore that $dR = dE/k(E)$, where $k(E)$ represents the ionization loss of a proton of energy E. One then obtains for $j^{(p)}(E,x)$ the expression:

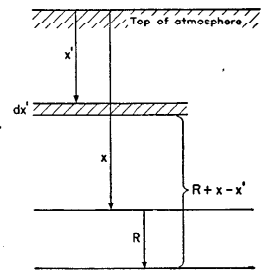

Fig. 8.14.1. Illustrating the computation of the proton spectrum in the atmosphere.

$$k(E)j^{(p)}(E,x) = \int_0^x k(E')s^{(p)}(E',x')e^{-(x-x')/L_c}\,dx', \tag{2}$$

where E' is related to E, x, and x' by the condition:

$$R(E') = R(E) + x - x'. \tag{3}$$

For kinetic energies smaller than about 0.5 Bev, $k(E)$ increases rapidly with decreasing energy. Since obviously $E' < E$, Eq. (2) shows that ionization loss strongly depletes that low-energy end of the proton spectrum, as already pointed out in § 8.5.

Assume that the dependence of $s^{(p)}(E,x)$ on energy is the same at all depths, and that the dependence of $s^{(p)}(E,x)$ on depth may be approximated by an exponential function: $\exp(-x/L)$. One can then write Eq. (2) as follows:

$$k(E)j^{(p)}(E,x) = \int_0^x k(E')s^{(p)}(E',x)e^{-(x-x')[(1/L_c)-(1/L)]}\,dx'. \tag{4}$$

For sufficiently small values of E', the quantity $s^{(p)}(E',x)$ is a rapidly decreasing function of E', and since E' increases with decreasing x', it is a rapidly increasing function of x'. Physically this means that most of the protons of moderate energy observed at the depth x have been produced at depths close to x. The exponential term in Eq. (4) represents the combined result of the two following partially compensating effects. As the depth x' of the production layer decreases, the rate of production of protons increases. At the same time, however, the distance $x-x'$ between the production layer and the observation point increases, thus increasing the chance that the produced protons may be absorbed by nuclear collisions

in the atmosphere before reaching the depth x. Therefore the exponential term varies slowly with x' and, on a first approximation, it may be taken as equal to one for all values of x' which contribute appreciably to the integral. One then obtains:

$$k(E)j^{(p)}(E,x) = \int_0^x k(E')s^{(p)}(E',x)\,dx',$$

or, since $dE' = -k(E')\,dx'$,

$$k(E)j^{(p)}(E,x) = \int_E^{E_m} s^{(p)}(E',x)\,dE', \tag{5}$$

where the upper limit of the integral, E_m, is defined by the equation:

$$R(E_m) = R(E) + x. \tag{6}$$

Observations by means of photographic emulsions at an atmospheric depth of 50 g cm^{-2} have yielded the production spectrum of protons shown in Fig. 8.10.3. Unfortunately the secondary protons recorded in photographic emulsions arise mainly from interactions with heavy nuclei, whereas the protons in the atmosphere arise from interactions with light nuclei. We shall neglect the possible difference between the production spectra of protons coming from heavy and light nuclei and represent the production spectrum by the function:

$$s^{(p)}(E,x) = \frac{Ae^{-x/L}}{(50+E)^2}, \tag{7}$$

where A is a constant and E is measured in Mev. In the energy region extending from 50 Mev to 1,000 Mev this function fits the experimental points shown in Fig. 8.10.3 within the experimental errors.

By means of Eq. (7) we then obtain the following expression for the proton intensity $j^{(p)}(E,x)$:

$$j^{(p)}(E,x) = \frac{Ae^{-x/L}}{k(E)}\frac{E_m - E}{(50+E)(50+E_m)}. \tag{8}$$

For comparison, one may compute the differential intensity of neutrons, under the assumption that the production spectrum of neutrons is identical to that of protons and is therefore given by Eq. (7). With this production spectrum Eq. (1) yields:

$$j^{(n)}(E,x) = \frac{Ae^{-x/L}}{(50+E)^2}\int_0^x e^{-(x-x')(1/L_c - 1/L)}\,dx. \tag{9}$$

In agreement with the approximation made in the computation of the proton intensities we assume that the exponential term in Eq. (9) may be taken equal to one for all values of x.* Equation (9) then becomes:

* Note that this assumption has a clear justification in the case of low-energy protons, which cannot come from very far because of their rapid absorption by ionization loss. In the case of neutrons or of high-energy protons, it is justified only if $L_c \sim L$, i.e., if the collision mean free path of the secondary particles is not very different from the absorption thickness of the primary radiation (§5.15). Moreover, the expression for the proton spectrum should include an additional term representing the primary protons (whose minimum energy is determined by their geomagnetic cutoff) attenuated in their passage through the atmosphere.

$$j^{(n)}(E,x) = \frac{Ax}{(50+E)^2}e^{-x/L}. \tag{10}$$

Figure 2 shows the quantities $j^{(p)}(E,x)$ and $j^{(n)}(E,x)$ as functions of E for $x = 700$ g cm^{-2}. One sees that the two functions slowly approach one another as the energy increases.

We cannot trust our computations to give the exact value of the energy at which the differential proton spectrum has its maximum, because the position of this maximum is quite sensitive to the assumed production spectrum. However, the general features of the spectra shown in Fig. 2

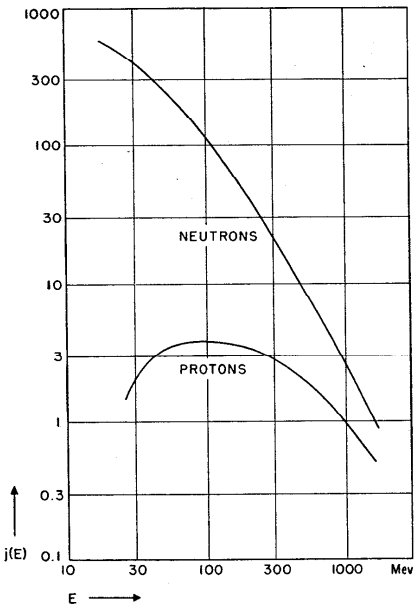

Fig. 8.14.2. The computed differential energy spectra of protons and neutrons in the atmosphere at 700 g cm^{-2} (ordinate in arbitrary units).

are probably correct. In particular this figure shows that, in the low-energy region, $j^{(p)}(E,x)$ decreases rapidly with decreasing energy, as predicted from qualitative considerations.

For energies above 1,000 Mev there are no direct determinations of the production spectrum of protons. The production spectrum given by Eq. (7) certainly cannot be extrapolated to $E = \infty$ because it would yield a diverging value for the total energy of the secondary protons. For lack of better information, and with the full realization that we are making an arbitrary choice that future experiments may confirm or disprove, we shall assume [with Camerini and his collaborators (CU50)] that the differential production spectra of protons and neutrons are represented by Eq. (7) for energies smaller than 1,000 Mev and are represented by power functions with exponent -2.5 for energies greater than 1,000 Mev. From this assumption and from our previous results it follows that the differential intensities of protons and neutrons at high energies are also approximately proportional to $E^{-2.5}$.

8.15. ***The propagation of N-rays through the atmosphere.*** In the preceding sections we have analyzed the experimental information concerning the nature of the cosmic-ray particles that undergo nuclear interactions and of the secondary particles resulting from such interactions. We now turn our attention to the quantitative problem of the cross-sections for collisions between cosmic-ray particles and atomic nuclei.

Among the experimental results that have a bearing upon this important problem, one of the best-established is the curve giving the rate of occurrence of high-energy nuclear interactions as a function of atmospheric depth (see Fig. 8.4.3).

It is convenient to introduce at this point the expression "N-rays" as an abbreviation for "cosmic-ray particles that produce nuclear interactions." Thus N-rays include protons, neutrons, and π-mesons. We do not consider here the topmost layers of the atmosphere where high-energy α-particles and heavier nuclei are present in considerable numbers.

Within the experimental uncertainties the atmospheric absorption curve of high-energy N-rays is represented by an exponential function: $\exp(-x/L)$ with $L \approx 120$ g cm^{-2}. An exponential absorption curve is often indicative of a "catastrophic" absorption process, i.e., one in which the interacting particles completely disappear. When this is the case, the quantity L, which we may generically define as the *absorption thickness*, represents the collision mean free path. Such an interpretation of cosmic-ray data would yield a value of about 120 g cm^{-2} for the collision mean free path in air of the high-energy nucleons that are mainly responsible for the observed nuclear interactions.

This point of view undoubtedly is an oversimplification of the actual situation. Cosmic-ray nucleons have a continuous energy distribution whose upper limit has not yet been discovered. Nuclear interactions

of high-energy nucleons can certainly produce secondary nucleons and π-mesons capable of giving rise to nuclear interactions of the type recorded by our instruments. The production of these secondary particles partially compensates for the absorption of the primary particles and thus tends to decrease the slope of the absorption curve.

If secondary production of interacting particles plays an important role, the atmospheric absorption curve is no longer by necessity an exponential, even if the collision mean free path is independent of energy. In this case, actually, the shape of the absorption curve depends not only on the cross-sections for nuclear interactions of the various interacting particles (primary and secondary), but also on their energy spectrum. Thus, one might consider the approximately exponential character of the absorption curve as an argument against the assumption that the production of secondary particles has a considerable influence upon the shape of this curve. This argument, however, is not well grounded. As we have seen, the shower theory affords examples of complex radiations that are absorbed exponentially even though reproduction plays a very important role in their propagation through matter. Indeed, Heitler and Janossy (HtW49) have developed a theory for the propagation of N-rays through matter which reconciles the exponential character of the absorption curve and the experimental value of the absorption thickness with an assumed collision mean free path equal to the geometric mean free path. Thus, before analyzing the problem in more detail, one can only conclude that the value of the collision mean free path of high-energy nucleons in air lies between the observed absorption thickness (120 g cm^{-2}) and the geometric mean free path (68 g cm^{-2}).*

In what follows we shall discuss from a more quantitative standpoint the relation between the absorption thickness of N-rays and the collision mean free path of high-energy nucleons in air. For this purpose it may be useful to reconsider the definitions of some of the concepts that enter into this discussion.

Each particular detector selects a different group of N-rays, namely those capable of producing nuclear interactions of the type that the detector will record (e.g., a shower of penetrating particles, a star with a given minimum number of prongs, etc.). Consider, for simplicity, a detector selecting vertical N-rays. The counting rate observed at the atmospheric depth x is given, in general, by an expression of the type:

$$C(x) = \sum_i \int_0^\infty j^{(i)}(E,x) g^{(i)}(E)\, dE, \tag{1}$$

where $j^{(i)}(E,x)$ represents the differential intensity of N-rays of a certain kind (protons, neutrons, π-mesons) at the depth x and $g^{(i)}(E)$ is an instrumental factor describing the efficiency for the detection of an N-particle of type i and of energy E. Equation (1)

* Neglected here is the fact that the N-rays recorded by a penetrating-shower detector are not exactly vertical, so that the average distance travelled by the detected particles in a given layer of air is slightly greater than the thickness of this layer. This effect may result in a slight underestimate of the absorption thickness.

may be regarded as an exact definition of what is usually called the "absorption curve" of N-rays. The validity of this definition, of course, is not limited to the case of atmospheric absorption, which forms the subject of the present section.

As a general definition of the absorption thickness L we may use the equation:

$$\frac{1}{L} = -\frac{d(\ln C)}{dx}. \tag{2}$$

In the case of an exponential absorption:

$$C(x) = \text{const.} \cdot e^{-x/L}, \tag{3}$$

the absorption thickness is independent of x and coincides with the coefficient L appearing in Eq. (3). Thus it represents the absorber thickness in which the counting rate decreases by a factor of e.

The function $C(x)$ depends, of course, on the selective efficiency of the detector for different groups of N-rays. One often assumes that $C(x)$ is proportional to the total number of N-rays of energy greater than a certain value, E_0, characteristic of the detecting instrument. This is equivalent to the assumption that each of the functions $g^{(i)}(E)$ may be approximated by a step function: $g^{(i)}(E) = 0$ for $E < E_0$, $g^{(i)}(E) = K$ (K = const) for $E > E_0$. $C(x)$ is then given by the equation:

$$C(x) = K\sum_i J^{(i)}(E_0,x), \tag{4}$$

where:

$$J^{(i)}(E_0,x) = \int_{E_0}^{\infty} j^{(i)}(E,x)\,dE \tag{5}$$

is the "integral spectrum" of the i-component of N-rays.

As a first step we wish to discuss the influence of π-mesons upon the atmospheric absorption curve of N-rays.

Pi-mesons are produced primarily by nucleons: we shall neglect those π-mesons that may be produced by nuclear interactions of other π-mesons. The rate of production of π-mesons, per unit linear distance, increases in proportion to the density of air, whereas their rate of decay is independent of density. Therefore the number of π-mesons, relative to that of nucleons, is proportional to the density of air. Under the approximation of an isothermal atmosphere, the density of air is proportional to the atmospheric depth x. The counting rate, $C^{(\pi)}(x)$, due to the nuclear interactions of π-mesons is thus related to the counting rate, $C^{(p,n)}(x)$, due to nuclear interactions of protons and neutrons by an equation of the type:

$$C^{(\pi)}(x) = AxC^{(p,n)}(x), \tag{6}$$

where A is a constant. The total counting rate is:

$$C(x) = C^{(p,n)}(x) + C^{(\pi)}(x) = C^{(p,n)}(x)(1 + Ax). \tag{7}$$

Notice that if the function $C^{(p,n)}(x)$ has an approximately exponential behavior, the function $C(x)$ has also an approximately exponential behavior over a wide range of atmospheric depth. Thus, with the limited accuracy of the experimental determinations, the only noticeable effect of meson production will be a change in the absorption thickness. If L represents the observed absorption thickness and $L^{(p,n)}$ the absorption thickness of the nucleonic component alone, Eq. (2) together with Eq. (7) yields the following relation:

$$\frac{1}{L} = \frac{1}{L^{(p,n)}} - \frac{A}{1 + Ax} = \frac{1}{L^{(p,n)}} - \frac{1}{x}\frac{C^{(\pi)}(x)}{C(x)}. \tag{8}$$

This equation shows that $L^{(p,n)} < L$. However it also shows that the difference between these two quantities cannot be large, at least near sea level. Indeed, since $C^{(\pi)} < C$, Eq. (8) yields, as an absolute minimum for the value of $L^{(p,n)}$:

$$L^{(p,n)} = \frac{Lx}{L + x}.$$

Near sea level, as well as at the higher elevations, $L \approx 120$ g cm^{-2}. Therefore one concludes that $L^{(p,n)}$ must be greater than about 107 g cm^{-2}.

In the above discussion *we have implicitly assumed that the composition of the nucleonic component does not change with depth.* General arguments then show that the absorption curve of the nucleonic component is necessarily exponential (see § 5.6) and so is the production curve of the π-mesons arising from the interactions of the nucleonic component.

Let $L_c^{(\pi)}$ represent the collision mean free path of π-mesons in the atmosphere. Assume that $L_c^{(\pi)}$ is independent of energy and neglect, as before, the production of secondary π-mesons in the nuclear interactions of π-mesons. Assume further that the atmosphere is isothermal. The linear vertical distance, z, between two levels at the atmospheric depths x_1 and x respectively ($x_1 < x$) is then given by the equation:

$$\frac{x}{x_1} = e^{z/z_0}, \tag{9}$$

where z_0 is a constant (see Appendix 6). If ionization loss is negligible, the probability that a π-meson of momentum p, produced at the depth x_1, reaches the depth x without disintegrating is:

$$e^{-z/z_d} = \left(\frac{x_1}{x}\right)^{z_0/z_d} = \left(\frac{x_1}{x}\right)^{z_0 m_\pi/\tau_\pi p}, \tag{10}$$

where z_d is the mean distance before decay (see Eq. (4.7.1), m_π is the mass, and τ_π is the mean life of the π-meson. The probability that the same meson escapes nuclear collisions is $\exp\,[-(x - x_1)/L_c^{(\pi)}]$.

Let $s^{(\pi)}(p,x)$ represent the differential production spectrum of π-mesons (with the momentum p as a variable) and let $j^{(\pi)}(p,x)$ represent the differential intensity of the π-mesons reaching the depth x (again with the momentum p as a variable). The considerations developed above yield the following equation:

$$j^{(\pi)}(p,x) = \int_0^x s^{(\pi)}(p,x_1)\left(\frac{x_1}{x}\right)^{z_0/z_d} e^{-(x-x_1)/L_c^{(\pi)}}\,dx_1. \tag{11}$$

If one now remembers that $s^{(\pi)}(p,x)$ is an exponential function of x, characterized by the same absorption thickness, $L^{(p,n)}$, that characterizes the absorption curve of the nucleonic component, one can write Eq. (11) in the following form:

$$j^{(\pi)}(p,x) = s^{(\pi)}(p,x)\int_0^x \left(\frac{x_1}{x}\right)^{z_0/z_d} e^{-(x-x_1)/L'}\,dx_1, \tag{12}$$

where

$$\frac{1}{L'} = \frac{1}{L_c^{(\pi)}} - \frac{1}{L^{(p,n)}}. \tag{13}$$

The quantity z_0 varies between $6.4 \cdot 10^5$ cm and $8 \cdot 10^5$ cm through the atmosphere (see Appendix 6). Unless p is exceedingly large, $z_0/z_d = z_0 m_\pi/\tau_\pi p$ is a large number. For example, when p is of the order of 10^{10} ev/c, z_0/z_d is of the order of 12. Thus $(x_1/x)^{z_0/z_d}$ is appreciably different from zero only when x_1 is very close to x and, on a

first approximation, one may consider the exponential term in Eq. (12) as equal to one. One then obtains:

$$j^{(\pi)}(p,x) = s^{(\pi)}(p,x)\,\frac{c_d L}{z_0 + z_d},$$

or, if one neglects z_d in the denominator:

$$j^{(\pi)}(p,x) = s^{(\pi)}(p,x)\,\frac{z_d}{z_0}\,x = s^{(\pi)}(p,x)\,\frac{\tau_\pi p}{z_0 m_\pi}\,x. \tag{14}$$

Since the rate of production of π-mesons, $s^{(\pi)}(p,x)$, is proportional to the intensity of the nucleonic component, Eq. (14) confirms the general relation expressed by Eq. (6) and determines the constant that appears in this equation.

If one avoids the approximations made in the derivations of Eq. (14) from Eq. (12), one obtains for $j^{(\pi)}(p,x)$ the expression:

$$j^{(\pi)}(p,x) = s^{(\pi)}(p,x)\,\frac{\tau_\pi p}{z_0 m_\pi}\,x\Lambda, \tag{15}$$

where Λ is a correction factor whose values are given in Fig. 1 in terms of the variables $y = x/L'$ and $h = z_0 m_\pi/\tau_\pi p$.

We wish to discuss, next, the effect of the reproduction of high-energy nucleons on the absorption curve of the nucleonic component in the atmosphere.

There is no doubt that high-energy nucleons are among the products of nuclear interactions occurring in the atmosphere. Indeed the general principles discussed in § 8.6 rule out the possibility that high-energy nucleons, colliding with other nucleons, may come to rest and expend all of their kinetic energy in the production of mesons.

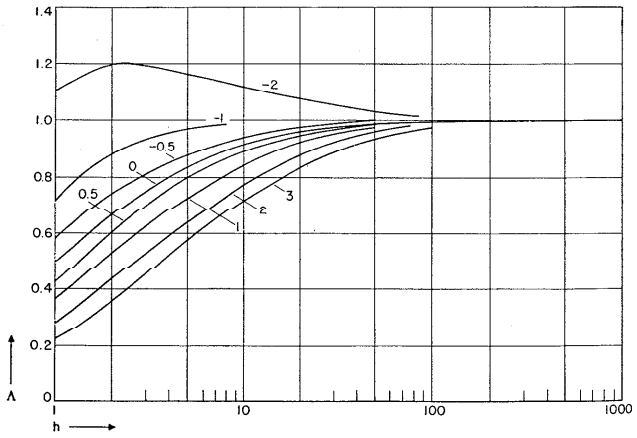

Fig. 8.15.1. The correction factor, $\Lambda(y,h)$, to the expression for the π-meson differential spectrum, Eq. (8.15.15), plotted as a function of $h = z_0 m_\pi/\tau_\pi p$. The numbers attached to the curves are the values of $y = x/L'$. (Unpublished computations by M. Annis.)

One may compute a minimum value for the reproduction factor by assuming that whenever a moving nucleon collides with a nucleon at rest, the two nucleons come to rest *in the center-of-mass system* and all of the kinetic energy available in this system goes into the production of mesons.* Thus, for each nucleon of a certain energy, E', that disappears from the incident beam two nucleons of lower energy, E, appear. Between E and E' there exists the relation [see Eq. (8.6.1)]:

$$E' = 4E\left[1 + \frac{E}{2Mc^2}\right]. \tag{16}$$

Let $J(E,x)$ represent the number of nucleons with energy greater than E in the incident radiation. If the collision mean free path is independent of energy, the reproduction factor, $f(E)$, is given by the equation:

$$f(E) = \frac{2J(E',x)}{J(E,x)}, \tag{17}$$

where E' and E are related to one another by Eq. (16). By reproduction factor we understand here the ratio between the number of nucleons above a certain energy that are produced and the number of nucleons above the same energy that disappear as a result of collisions between the incident nucleons and nucleons of the target nuclei.

If we assume that $J(E,x)$ obeys a power law with exponent -1.5 (see § 8.14), we obtain from Eqs. (16) and (17):

$$f(E) = 2\left(\frac{E'}{E}\right)^{-1.5} = \frac{1}{4}\left[1 + \frac{E}{2Mc^2}\right]^{-1.5}. \tag{18}$$

Penetrating-shower detectors, like the one used for the measurements on the altitude dependence of N-rays described in Fig. 8.4.3, have a threshold energy of at least several Bev. If we take $E = 5$ Bev for this threshold we find from Eq. (18) that the minimum value of the reproduction factor for the nucleons detected by the instrument in question is about 4 per cent.† From this result we conclude that, *if one postulates the maximum possible degree of inelasticity* in the nuclear collisions of cosmic-ray nucleons capable of producing penetrating showers, the difference between absorption thickness and collision mean free path of these nucleons amounts to only a few per cent.

We have not discussed thus far the ionization loss of protons. For the high energies considered here, the ionization loss is relatively unimportant. It slightly decreases the effect of reproduction and thus brings the absorption thickness somewhat closer to the collision mean free path.

In this connection, it may be worth while to point out that if protons and neutrons have the same collision mean free path, L_c, and if this is independent of energy, the ionization loss of protons will decrease the ratio of protons to neutrons (see § 8.14) but, in the lower atmosphere at least, it cannot make the absorption thickness of the nucleonic component shorter than L_c. In fact, in the lower atmosphere, an approximate condition of equilibrium exists between the various components of the N-radiation. Therefore the intensities of protons and neutrons decrease at about the same rate with increasing depth. On the other hand, the absorption thickness of neutrons, which undergo only nuclear interactions, cannot be shorter than L_c.

---

* For a detailed discussion of the propagation of N-rays through the atmosphere under the assumption of "maximum inelasticity," the reader may consult a paper by Milford and Foldy (MFJ51).

† The reproduction factor considered here is that relative to interactions with individual *nucleons*. The reproduction factor relative to interactions with *nuclei* is somewhat smaller, because of the possibility of multiple collisions within each nucleus.

From the preceding considerations it appears likely that the collision mean free path of high-energy nucleons in air is appreciably smaller than the observed absorption thickness of N-rays—even though, under extreme assumptions on the degree of inelasticity in nucleon-nucleon collisions, the difference between these two quantities could amount to only a few per cent. That the actual difference between L_c and L is greater than this minimum value, is confirmed by direct measurements of the collision mean free path of N-rays in light elements (see § 8.17).

As a very conservative upper limit for the collision mean free path of high-energy nucleons in air we shall take here $L_c = 110$ g cm^{-2}. Figure 7.7.2 then gives an upper limit $l_c \approx 4.3 \cdot 10^{-13}$ for the mean free path in nuclear matter and, correspondingly, a lower limit $\bar{\sigma} = 2.5 \cdot 10^{-26}$ cm^2 for the average cross-section for collisions between nucleons. It is interesting to note that this value of $\bar{\sigma}$ is not very different from the average cross-section for nucleon-nucleon collisions at about 300 Mev, as determined with artificially produced neutrons (see Fig. 7.3.1).

In § 8.4 we have shown that the atmospheric absorption curve obtained with nondirectional detectors sensitive to all N-rays with more than about 100 Mev energy is somewhat flatter than the absorption curve obtained with a penetrating shower detector selecting vertical N-rays of higher energy. The discrepancy is even greater than it appears to be from a direct comparison of the two curves, because, other conditions being equal, a nondirectional detector should give a *steeper* absorption curve than a directional detector (see § 8.4). It is thus fairly certain that the absorption thickness of low-energy N-rays in air is appreciably greater than the absorption thickness of high-energy N-rays.

However, it is quite possible that this energy dependence of the absorption thickness is not due to an energy dependence of the collision mean free path but rather to an increase with decreasing energy in the rate of reproduction of N-rays. For example, at energies where meson production is an impossible or an unlikely event, a neutron or proton may often traverse a nucleus losing only a moderate fraction of its energy.

The theoretical analysis of the propagation of low-energy N-rays through the atmosphere is very difficult. One of the many complicating factors is the necessity of taking into account ionization losses of protons, which plays only a minor role in the propagation of high-energy N-rays. We shall not attempt here to discuss this question in any detail but we refer the reader to the papers of Ferretti (FB49), of Messel and Ritson (MH50.1), of Messel (MH51.1; MH51.2), and of Budini and Dalla Porta (BdP50).

8.16. ***The absorption of N-rays in condensed matter.*** The interpretation of absorption measurements of the N component in condensed matter is difficult because of the intrinsic complexity of the phenomena involved and is often complicated further by instrumental factors.

It has not been possible, as yet, to extract from these measurements unambiguous results of a fundamental character and for this reason we intend to discuss the absorption measurements of N-rays in condensed matter much more briefly than the absorption measurements of N-rays in air. As cosmic rays pass from air to a condensed absorber, the mean free path for nuclear interaction changes and so does the amount of ionization loss of protons in one mean free path. Most important of all, the number of π-mesons relative to that of nucleons increases greatly because very few π-mesons decay in flight while traveling through condensed matter. Since, to the best of our knowledge, π-mesons and nucleons have comparable cross-sections for nuclear collisions, a large fraction of the interactions observed under a condensed absorber must be due to π-mesons.

In the atmosphere the various components of N-rays are probably in a condition of approximate equilibrium with one another. The above considerations show that this equilibrium condition is perturbed when the radiation enters a condensed absorber. Presumably after a sufficient thickness of absorber the radiation will reach a new equilibrium condition, characterized by a much larger proportion of π-mesons relative to nucleons. In the transition layer the intensity of N-rays will decrease more slowly than at larger absorber thicknesses, and perhaps even increase at first, go through a maximum, and then decrease again.

In discussing observations dealing with nuclear interactions of comparatively low energy one must also consider the possibility that a small but not negligible number of these interactions may be due to photons. Photons, of course, exhibit pronounced transition effects in the passage from one absorber to another of different atomic number.

Various authors have reported absorption measurements of the star-producing radiation in condensed matter, made by means of photographic emulsions.

Harding and his collaborators (HJB49.4) found in ice an approximately exponential absorption with an absorption thickness of 200 g cm^{-2}. With lead as an absorber, Bernardini and his collaborators (BG49) found an increase in the rate of occurrence of stars in the first several centimeters, followed by an approximately exponential decrease corresponding to an absorption thickness of about 300 g cm^{-2}. The same authors found in aluminum an approximately exponential absorption with an absorption thickness of about 200 g cm^{-2}. Measurements of George and Jason (GEP49.2) gave an absorption thickness of 310 ± 20 g cm^{-2} in lead. These measurements, however, were not accurate enough to check the results of Bernardini concerning the presence of a maximum at small lead thicknesses. Measurements of Barton, George, and Jason (BJC51) with carbon gave an absorption thickness of 166 ± 7 g cm^{-2}.

In general the absorption of the N-component in condensed matter, as measured by the various experimenters, appears to be somewhat smaller

than one would expect from the known absorption in air if one disregards the contribution of π-mesons to the N-component in condensed matter. In fact Barton and his collaborators interpreted their results as evidence for the presence of π-mesons among N-rays observed under carbon. It is, however, doubtful as to whether one can attribute to π-mesons the maximum in the transition curve found by Bernardini and his collaborators [for an alternate tentative explanation of this maximum, see ref. (DN50)].

The absorption of the N-component in condensed absorbers was also investigated by means of pulse ionization chambers, often in coincidence with trays of Geiger-Mueller tubes (FEF49; BHS49; RRH50). The experimental arrangements used in these experiments were of the general type illustrated in Fig. 8.3.3. The experimenters measured coincidences between the Geiger-Mueller tray and the ionization chamber with a fixed amount of lead immediately above the ionization chamber and with additional absorbers of various thicknesses either above or below the Geiger-Mueller tray.

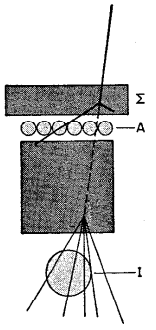

Fig. 8.16.1. The effect of "geometric coherence" on absorption measurements of N-rays in solid matter. A neutron produced in the absorber Σ undergoes a secondary interaction that gives a pulse in the ionization chamber, I, while an ionizing particle produced simultaneously with the neutron discharges the Geiger-Mueller tray A.

The ionization-chamber method is superior to the photographic-plate method because it yields greater statistical accuracy. It also selects N-rays of greater energy. However, it suffers from one serious disadvantage in that the detection efficiency depends on the "geometric coherence" of the particles to be recorded. Thus an N-particle emerging from the condensed absorber above the Geiger-Mueller tubes has a different probability of being detected depending on whether it has traversed the absorber or has been produced in the absorber. No such difference exists if the absorber is air instead of condensed matter.

This point may be clarified with the following example. Consider the experimental arrangement shown in Fig. 1. A neutron produced in the solid absorber placed above the Geiger-Mueller tray may discharge the ionization chamber by interacting in the lead immediately above it, while an ionizing particle produced simultaneously with the neutron in the primary interaction may discharge the Geiger-Mueller tray. In this case the neutron will be recorded. Consider, instead, a neutron projected through the instrument by a similar interaction occurring in the atmosphere. Because of the small density of air, the point of origin of this interaction will, on the average, be far above the instrument. In this case the neutron has a negligible chance of being recorded because, in general, it will not arrive upon the detecting instrument accompanied by the ionizing particles that may have been produced simultaneously with it.

Another disadvantage of the ionization chamber is that, in addition to nuclear interactions, it also records electronic showers produced by electromagnetic interactions of μ-mesons. If one tries to exclude these events (for example, by requiring the presence of several penetrating particles among the products of the interactions) one thereby increases the disturbing influence of the geometric coherence discussed above. The reader may consult ref. (RRH50) for a detailed discussion of these effects.

As an illustration of the ionization chamber method, Fig. 3 shows some of the results of absorption measurements made by Rediker at 3,260 meters altitude with the experimental arrangement sketched in Fig. 2. These results have been corrected for secondary effects of μ-mesons.

As mentioned repeatedly the absorption curve of high-energy N-rays in air is approximately exponential with an absorption thickness $L \approx 120$

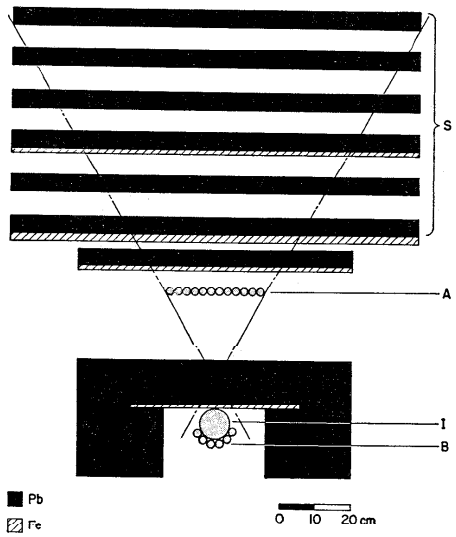

Fig. 8.16.2. Experimental arrangement used by Rediker to measure the absorption of N-rays in condensed matter (RRH50). The recorded event was a coincidence (AIB) between the Geiger-Mueller trays A and B, and the ionization chamber I. The ionization chamber was 7.5 cm in diameter, 53 cm long, and filled with argon at 7 atmospheres pressure. The bias was set at 1.6 Mev. The lead absorber, S, was subdivided into separate layers with wood spacers.

g cm^{-2}. If one neglects ionization losses of protons (which are comparatively unimportant for the high-energy particles detected in the experiment under discussion) and *if one were to assume that π-mesons do not contribute to the observed interactions*, one would conclude that the absorption curve of the N-component in lead is also an exponential, and one would obtain from Fig. 7.7.2 a value of about 200 g cm^{-2} for the corresponding absorption thickness.* This absorption curve is shown by the dotted line in Fig. 3. It is very different from the experimental absorption curve and one is tempted to ascribe the discrepancy to the presence of π-mesons among N-rays emerging from lead. Unfortunately the uncertainty concerning the effects of geometric coherence does not allow one to regard this conclusion as final.

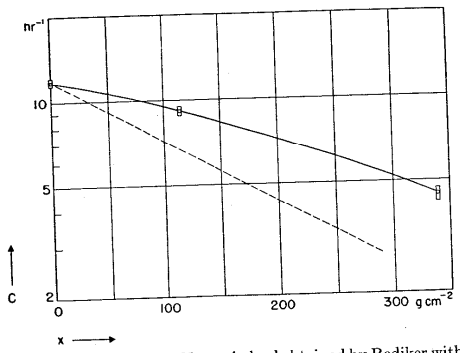

Fig. 8.16.3. Absorption curve of N-rays in lead obtained by Rediker with the experimental arrangement shown in Fig. 8.16.2. The abscissa is the thickness, x, of the absorber, S, placed above the instrument. The ordinate is the rate, C, of coincidences between the Geiger-Mueller tray A, the ionization chamber I and the Geiger-Mueller tray B. The ionization chamber had a diameter of 7.5 cm and was filled with argon at 7 atmospheres. The minimum pulse required corresponded to a dissipation of 1.6 Mev in the chamber. The data were corrected for secondary effects of μ-mesons. The dashed line represents an exponential absorption curve with absorption thickness L_a = 200 g cm^{-2}.

8.17. ***The collision mean free path of N-rays.*** The collision mean free path is a fundamentally simpler quantity than the absorption thickness discussed in the two preceding sections. As repeatedly mentioned, it

* The arguments developed in § 8.6 show that one may use Fig. 7.7.3 to determine the relation between absorption thickness of N-rays in different materials even when the absorption thickness differs from the collision mean free path; i.e., when reproduction phenomena are important. This is true under the assumption that absorption and reproduction of N-rays result entirely from nuclear interactions and under the approximation implicit in the concept of "thickness of nuclear matter" (see §§ 7.7 and 8.6 for a discussion of this approximation).

represents the mean thickness (in g cm^{-2}) traversed by a particle before it undergoes a nuclear interaction. In this section we shall describe briefly the methods used by various experimenters for determining the collision mean free path, L_c, of high-energy N-rays present in the atmosphere.

We shall assume that this mean free path is the same for all N-rays capable of producing the observed nuclear events. If it is not, the results obtained will represent some average value of L_c for the particles under consideration.

(a) The first method is based upon an analysis of the "transition curves" for penetrating showers (see § 8.2); i.e., of the curves giving the rate of occurrence of coincidences in a penetrating-shower detector as a function of the thickness of the producing layer placed upon it. The experimental arrangements used for the measurements of the transition curves are of the type shown in Fig. 8.2.3 where T indicates the producing layer. Examples of the transition curves for "local" penetrating showers (as distinguished from "extensive" penetrating showers) are given in Figs. 8.2.7 and 8.2.9.

Let $C(x)$ be the counting rate recorded with a producing layer of thickness x. Suppose that an infinitesimal layer, dx, is added *above* the layer x. The probability for an N-particle to undergo a nuclear interaction in dx is dx/L_c. Therefore addition of the layer dx decreases the number of coincidences due to particles that undergo their first interaction in the layer x by an amount equal to $C(x)\,dx/L_c$.

On the other hand the secondary particles produced in the nuclear interactions that occur in dx have a certain probability of producing a coincidence in the penetrating shower detector, either directly or by interacting again in the material below. If this probability were independent of the thickness, x, of the pre-existing layer, the increase in counting rate due to the interactions occurring in dx would have an expression of the type: $A\,dx/L_c$, where A is a constant. One would then obtain the following differential equation for the counting rate:

$$\frac{dC(x)}{dx} = -\frac{C(x)}{L_c} + \frac{A}{L_c}. \tag{1}$$

The solution of this equation is:

$$C(x) = C(0)e^{-x/L_c} + A(1 - e^{-x/L_c}), \tag{2}$$

where $C(0)$ represents the counting rate observed with no producing layer above the penetrating-shower detector (in this case the upper tray of counters is discharged by particles ejected in the backward direction; see § 8.2).

However, the assumption made is incorrect; indeed, the probability for the secondary particles arising in dx to produce a coincidence depends on x for two different reasons: (1) because the secondary particles emerging

from the nuclear interactions lose energy and may undergo further nuclear interactions on traversing the thickness x; (2) because, even if the secondary particles traversed the layer x unaffected, the probability of their producing a coincidence would still depend on the linear distance of their point of origin from the penetrating-shower detector.

George and Jason (GEP50.2) have investigated the geometric effect (No. 2 above) by measuring the counting rate with a producing layer of constant thickness placed at different distances from the penetrating-shower detector. They have then analyzed the transition curves obtained in their experiments at 3,450 meters (see Fig. 8.2.9) by using the geometric correction determined experimentally and *by assuming that effect No. 1 is negligible.* From this analysis they have obtained the following values for the collision mean free paths:

in lead:	$L_c = 180 \pm 40$ g cm^{-2};
in aluminum:	$L_c = 85 \pm 15$ g cm^{-2}:
in paraffin:	$L_c \approx 80$ g cm^{-2}.

As already pointed out, these results are based upon the assumption that the probability of recording a nuclear interaction occurring above a penetrating-shower detector is independent of the amount of material placed between the origin of the nuclear interaction and the detector. In the opinion of the writer, this assumption is questionable and it is thus difficult to determine how much significance one can attach to the values of the collision mean free path found by the method discussed above.

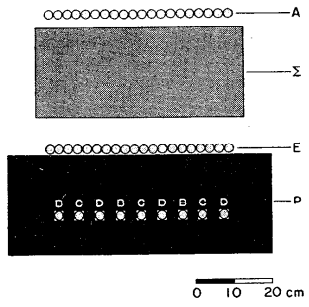

Fig. 8.17.1 Experimental arrangement used by Cocconi for the measurement of the collision mean free path of ionizing N-rays (CG49.3).

(b) The principle of the second method is illustrated in Fig. 1 reproduced from a paper by Cocconi (CG49.3). In this figure, P represents a penetrating-shower detector consisting of a group of Geiger-Mueller tubes (marked B,C,D) embedded in a large block of lead. A and E are two additional trays of Geiger-Mueller tubes. Σ represents an absorber of variable thickness. Electronic circuits select events that cause the discharge of at least one counter in tray A, at least one counter in each of the groups B, C, D, and of one and only one counter in tray E (coincidences $ABCDE_1$).

Without any absorber in Σ, the instrument records ionizing N-rays that traverse tray A and E and then produce in the lead a nuclear interaction whose secondary particles discharge counters B, C, D (we neglect here the small number of nuclear events produced by neutrons and whose back-scattered secondary particles go through trays A and E, discharging only one tube in the latter tray). With an absorber of thickness x in Σ, the fraction of the incident N-rays that arrives upon the penetrating-shower detector P without previous interaction equals exp $(-x/L_c)$. Each of these particles has the same probability of being recorded as if the absorber were not present (see Fig. 2a). On the other hand, groups of

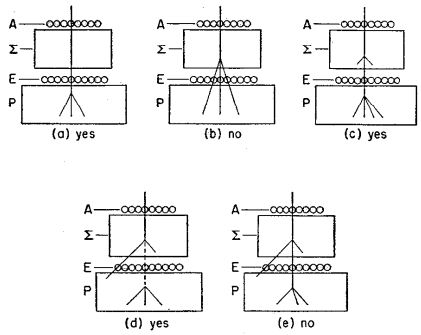

Fig. 8.17.2. Types of events that are recorded and types of events that are not recorded by the experimental arrangement shown in Fig. 8.17.1.

penetrating particles arising from nuclear interactions of N-rays in Σ cannot discharge counters B, C, and D without discharging more than one counter in tray E (Fig. 2b). Thus Σ acts exclusively as an absorber, in the sense that penetrating showers originating in Σ cannot give rise directly to the required $ABCDE_1$ coincidences.

However, an ionizing N-ray that undergoes an interaction in Σ may still be recorded. For example, the interaction may produce an ionizing particle that traverses tray E and then interacts again in P, discharging counters B, C, and D with its secondary products. This event will produce an $(ABCDE_1)$ coincidence if none of the other ionizing particles arising from the first interaction strikes tray E (see Fig. 2c). Or the first interaction may produce a neutral particle that interacts again in P and an ionizing particle that discharges one tube in tray E (Fig. 2d).

If the probability of events such as those described in Figs. 2c and 2d is negligible, then only those N-rays that fail to interact in the absorber Σ

can be detected and the counting rate, $C(x)$, varies with absorber thickness x according to the exponential law:

$$C(x) = C(0)e^{-x/L_c}. \tag{3}$$

If this probability is not negligible, then the logarithmic slope of the observed absorption curve, i.e., the quantity $-d[\ln C(x)]/dx$, is smaller than $1/L_c$. In other words, the experiment yields too large a value for the mean free path.

One should note that the probability of detection for a particle that has interacted in Σ depends critically upon the experimental arrangement. The probability is small if the absorber Σ is thin, so that most of the secondary products of the interactions occurring in Σ emerge from this absorber, and if Σ is close to E so that these products are likely to discharge more than one counter in this tray. The probability may be large if the above conditions are not verified.

In the discussion above, we have neglected the effect of ionization loss. In order to evaluate the magnitude of this effect we shall assume that all ionizing N-rays of energy greater than E have equal detection probability, so that the counting rate is proportional to the number, $J(E,x)$, of ionizing N-rays of energy greater than E that traverse the absorber x without interaction. For particles of relativistic velocities, the ionization loss per g cm^{-2} may be regarded as constant; let k be its value. As the absorber thickness is increased from x to $x + dx$ a number of particles equal to $-k\,(\partial J/\partial E)\,dx$ falls below the energy threshold E by ionization loss. By considering this effect together with that of nuclear interactions one obtains the following equation:

$$\frac{\partial J(E,x)}{\partial x} = -\frac{J(E,x)}{L_c} + k\frac{\partial J(E,x)}{\partial E}, \tag{4}$$

from which it follows:

$$-\frac{\partial[\ln J(E,x)]}{\partial x} = \frac{1}{L_c} - \frac{k}{E}\frac{\partial[\ln J(E,x)]}{\partial(\ln E)}. \tag{5}$$

The term on the left-hand side represents the inverse of the "apparent" mean free path; we shall call this quantity L_c'. If one approximates the dependence of J on E by a power function with exponent $-\alpha$, Eq. (5) yields:

$$\frac{1}{L_c'} = \frac{1}{L_c} + \frac{\alpha k}{E}. \tag{6}$$

One sees that the ionization loss makes the mean free path appear shorter than it actually is. Suppose for example that the absorber is lead, that L_c is identical to the geometric mean free path ($L_c = 164$ g cm^{-2}) and that the threshold energy of the penetrating-shower detector is $E = 5 \cdot 10^9$ ev. Equation (6), with $\alpha = 1.5$ (see § 8.14) and $k = 1.2 \cdot 10^6$ ev g^{-1} cm^2 (see § 2.9), then yields:

$$\frac{L_c - L_c'}{L_c'} = 0.07. \tag{7}$$

In the evaluation of the experimental results, one should consider still another source of error. The incident rays do not form a parallel beam and thus they traverse, on the average, an amount of matter greater than the actual absorber thickness. The corresponding correction is of the order of several per cent, but its exact value depends on the shape of the apparatus.

Several experimenters have reported the results of measurements based upon the principle described above (TJH49.1; CG49.1; CG49.3; WWD50.1; SK50; RRH50; WWD50.2). The numerical values of the mean free paths found in these measurements spread over a fairly wide range. Probably differences in the experimental arrangements are largely responsible for the observed discrepancies. As pointed out by Cocconi (CG49.3) it is also likely that a background due to electromagnetic interactions of μ-mesons may have affected some of the experimental results.

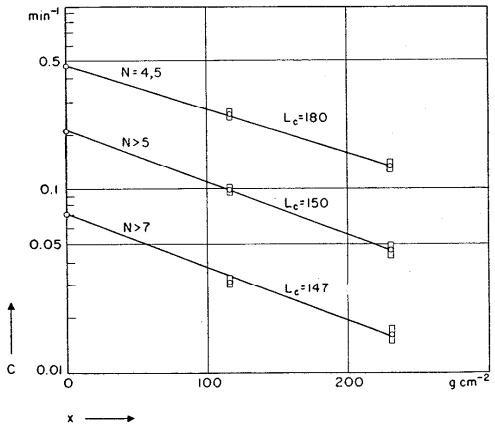

Fig. 8.17.3. Determination of the collision mean free path of N-rays in lead. The data were obtained with an experimental arrangement similar to that illustrated in Fig. 8.17.1 (C represents the counting rate, x the absorber thickness). The curves correspond to events discharging different numbers of counters, N, in the penetrating shower detector. [From Walker (WWD50.1).]

In general, one may say that experiments performed under conditions that minimize the effects of secondary interactions yield mean free paths *in lead* close to the geometric value of 164 g cm^{-2}. Thus Cocconi, at 3,260 meters altitude, after correcting for the meson background, found in lead an exponential absorption curve with a logarithmic slope corresponding to a collision mean free path of approximately 160 g cm^{-2} (CG49.3). At the same altitude, Walker (WWD50.1) found collision mean free paths in lead equal to 180 ± 10 g cm^{-2}, 150 ± 8 g cm^{-2}, and 147 ± 10 g cm^{-2} respectively by selecting events that discharged different numbers, N, of counters in his

penetrating shower arrangement ($N = 4$ or 5 in the first case, $N > 5$ in the second case, $N > 7$ in the third case). The experimental results of Walker are shown graphically in Fig. 3. According to these results the apparent mean free path decreases with increasing size of the penetrating shower and therefore, presumably, with increasing energy of the initiating particle. It is possible that this effect is due to a change in the effect of secondary interactions rather than to an energy dependence of the mean free path for nuclear collisions. Indeed, nuclear interactions capable of giving rise to secondary N-rays of greater energy are likely to result in more violent disintegrations and have probably greater chance of discharging more than one tube in tray E. If this is correct, the selection of high-energy nuclear events minimizes the difference between actual and apparent mean free path.

Sitte (SK50), again working at 3,260 meters altitude, found a collision mean free path in lead of 162 ± 10 g cm^{-2} for the primaries causing showers capable of penetrating 200 g cm^{-2} of lead, and a collision mean free path in lead of 196 ± 13 g cm^{-2} for the primaries causing showers capable of penetrating 100 g cm^{-2} of lead. These results, in agreement with those of Walker, quoted above, show that the apparent mean free path of N-rays decreases with energy. Finally Walker and his collaborators (WWD50.2), in another experiment performed at 4,260 meters altitude, found a collision mean free path in lead of about 157 g cm^{-2} (this value is corrected for the lack of parallelism of the incident radiation).

Cocconi (CG49.3) and Walker (WWD50.2) also measured the collision mean free path of ionizing N-rays in carbon and found values of about 100 g cm^{-2} and 81 ± 5 g cm^{-2} respectively. These values compare with a geometric mean free path of 63 g cm^{-2}. (Cocconi's value may need a correction of the order of 5 or 10 per cent to account for a small μ-meson background.)

Some of the measurements with lead discussed above, if taken at face value, yield a mean free path shorter than the assumed geometric mean free path (164 g cm^{-2}). One should note, however, that the statistical accuracy of the measurements is not very great. Moreover, some of the experimental results may need corrections to account for the ionization loss and for the lack of parallelism of the incident beam. Also the nuclear radii and, therefore, the geometric mean free paths are not known with great precision.

(c) The third method is designed to determine the collision mean free path of neutral N-rays (high-energy neutrons according to our interpretation). Rossi and Regener (RB40.3), Janossy and Rochester (JL43.1), Walker, Walker, and Greisen (WWD50.2), and Boehmer and Bridge (BHW51) have attacked this problem with experimental arrangements based upon the same principle, though different in their details. The first two experiments achieved little more than to demonstrate the existence

of neutral particles capable of producing penetrating showers and to show that these particles, because of their small absorption in lead, could not be photons. The last two experiments yielded quantitative data on the collision mean free path.

Figure 4 shows the arrangement used in the experiment of Boehmer and Bridge. A, B, C, D, and E are trays of Geiger-Mueller tubes. F,F are additional trays used to discriminate against air showers. The black areas represent lead. Σ represents an absorber of variable thickness. Electronic circuits select various kinds of coincidences and anti-coincidences, among which we wish to consider here specifically those coincidences

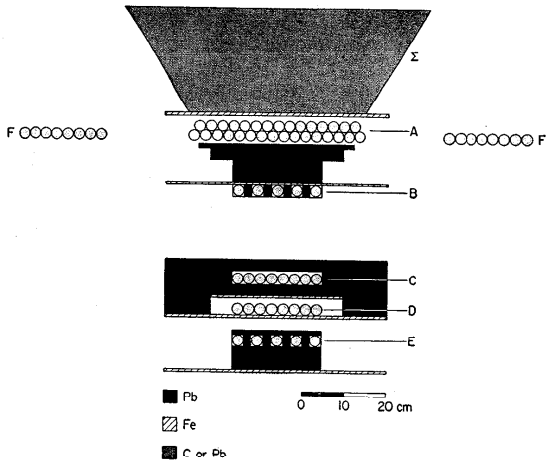

Fig. 8.17.4. Experimental arrangement used by Boehmer and Bridge to measure the collision mean free path of neutral N-rays (high-energy neutrons).

between trays B, C, D, E that involve the discharge of two or more tubes in each of trays B and E and are not accompanied by discharges in trays A or F (anti-coincidences $B_{\geq 2}CDE_{\geq 2} - AF$). These events are interpreted as due to high-energy neutrons traversing tray A undetected and then undergoing, in the lead between A and B, nuclear interactions whose secondary products produce coincidences $B_{\geq 2}CDE_{\geq 2}$.

With an absorber in position Σ, neutrons coming from the atmosphere and traversing the absorber without interactions have the same probability of being recorded as if the absorber had not been there. On the other hand, a high-energy neutron produced in Σ by the nuclear interaction of either a neutron or a charged N-ray may give rise to the required anti-

coincidence only if the ionizing particles that are usually produced simultaneously with the neutron fail to discharge tray A. This event is probably rare. One should therefore expect that the counting rate decrease with increasing absorber thickness according to the exponential function, $\exp(-x/L_c)$, where L_c is the collision mean free path of neutrons. Figure 5 shows the experimental results obtained with absorbers of carbon and lead. Within the experimental errors, the observed absorption curves are exponential. The corresponding mean free paths are about 220 g cm^{-2} in lead and 110 g cm^{-2} in carbon.

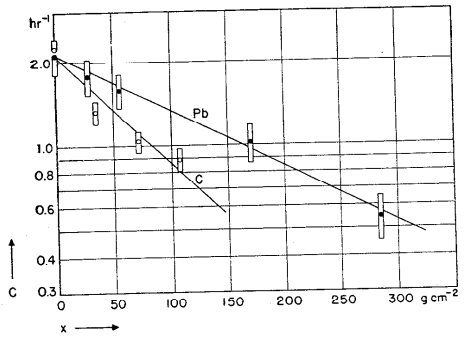

Fig. 8.17.5. Some of the experimental results obtained with the arrangement shown in Fig. 8.17.4. The abscissa represents the thickness x, in g cm^{-2}, of the absorber Σ (lead or carbon). The ordinate represents the counting rate, C, of anti-coincidences ($B_{\geq 2}CDE_{\geq 2} - AF$). The straight lines correspond to collision mean free paths L_c = 220 g cm^{-2} in lead, and L_c = 110 g cm^{-2} in carbon. [From H. W. Boehmer and H. S. Bridge, unpublished results.]

Similar measurements by Walker and his collaborators (WWD50.2) gave $L_c = 164 \pm 15$ g cm^{-2} in lead and $L_c = 80 \pm 7$ g cm^{-2} in carbon.

One sees that, within the experimental errors, the collision mean free paths of non-ionizing N-rays in lead or carbon are not significantly different from the collision mean free paths of ionizing N-rays in the same elements.

8.18. ***Experimental data on the relative cross-sections of different elements for nuclear interactions.*** Lovati, Mura, Salvini, and Tagliaferri (LA50), and Gregory and Tinlot (GBP51) used cloud chambers containing alternate plates of lead and of a light element (carbon and aluminum respectively) to investigate the dependence of the nuclear cross-section on atomic number. The experiment of Gregory and Tinlot has already been mentioned in § 8.9. In a first series of measurements these authors used a triggering arrangement selecting ionizing particles (see

Fig. 8.1.18c). As explained previously, most of the interacting particles so selected were protons with energies around several hundred Mev. The ratio between the numbers of interactions per g cm^{-2} of lead and aluminum was found to be 0.5 ± 0.12. This figure, which also represents the inverse ratio between the mean free paths in the two elements, does not appear unreasonable. For example a mean free path in nuclear matter $l_c = 4 \cdot 10^{-13}$ cm yields a ratio $L_{Al}/L_{Pb} \approx 0.6$ according to Fig. 7.7.2.

In a second series of measurements Gregory and Tinlot used a triggering arrangement selecting neutrons of a greater average energy than that of the protons selected in the previous experiment (see Fig. 8.1.18e). Again comparing equal masses of lead and aluminum they obtained the following results:

(a) A lead-to-aluminum ratio of 0.6 ± 0.15 for nuclear interactions giving rise to 1 or 2 secondary penetrating particles.

(b) A lead-to-aluminum ratio of 1.25 ± 0.25 for nuclear interactions giving rise to 3 or more penetrating particles.

Lovati and his collaborators, selecting nuclear events with 4 or more secondary penetrating particles, found a ratio of about 2.2 ± 1 between the rates of occurrence of these events in 1 g cm^{-2} of lead and in 1 g cm^{-2} of carbon respectively.

It thus appears that the probability per g cm^{-2} for the occurrence of nuclear events giving rise to many penetrating particles is an *increasing* function of the atomic mass number, A. On the other hand, the probability per g cm^{-2} for inelastic nuclear collisions of any kind is a *decreasing* function of A, according to our nuclear model. This follows simply from the fact that the number of nucleons per gram is the same in all substances and that if nuclear matter has constant density, the "shadow effect" makes a nucleon in a heavy nucleus less effective than one in a light nucleus. Indeed the lead-to-aluminum or the lead-to-carbon ratio for the total interaction probability should be considerably less than one unless the lead nucleus were very transparent.

One can easily explain the apparent contradiction by assuming that when a nucleon of several Bev energy or more interacts with a nucleus the average number of penetrating particles produced is an increasing function of A. This is, indeed, what one should anticipate if successive collisions within a single nucleus play an important role in the production of the secondary penetrating particles (π-mesons, protons).

Observations by means of "sandwich plates" also have contributed some preliminary information on the relative cross-sections of different nuclei for nuclear interactions of cosmic rays. As already mentioned (see §§ 4.12 and 8.1), sandwich plates are plates covered with alternate layers of normal emulsion and plain gelatine. With such plates it is possible to compare the number of stars originating in pure gelatine (containing only carbon, nitrogen, oxygen, and hydrogen) with the number of stars originating in

the normal emulsion (containing, in addition to the above elements, bromine, silver, and traces of iodine). From this comparison one can then estimate the ratio between the average cross-section of the light nuclei (C,N,O) and that of the heavy nuclei (mainly Br and Ag) for the star-producing radiation.

Preliminary experiments by Harding (HJB49.1) with the method outlined above gave a value slightly greater than geometric for the ratio of the cross-sections of light and heavy nuclei. We feel that it would be premature to attempt an interpretation of this result before it is substantiated by further observations.

8.19. ***Nuclear interactions of secondary particles arising from nuclear events.*** Pictures obtained with multiple-plate cloud chambers offer numerous examples of particles (either charged or neutral) that arise from nuclear interactions and undergo further nuclear interactions before escaping from the chamber (see § 8.1, Figs. 24, 26e, 27, 30, 31, 32). Similar multiple interactions are also observed, although more rarely, in photographic emulsions (see Fig. 8.1.8). From these observations one can determine the mean free path for nuclear interactions of the *charged* secondary particles produced in nuclear interactions by dividing the total thickness of matter that the secondary particles traverse by the total number of secondary events to which they give rise. In practice an accurate measurement of the mean free path by this method represents a difficult task. The gathering of statistically significant data is a very time-consuming process, especially in the case of observations with photographic emulsions. In cloud-chamber experiments, on the other hand, one must use great care in order not to miss nuclear events that occur inside one of the plates and whose secondary products fail to emerge from the plate into the sensitive volume of the chamber. A particle producing such an event may be mistaken for a particle coming to the end of its range in the plate, if one does not consider the specific ionization of the track above the plate carefully; or it may be mistaken for a particle going out of the illumination, if no stereoscopic pictures are available to locate the trajectory accurately in space [see, for example, ref. (BWW50)]. Most important of all, one must avoid, or correct for, any discrimination introduced by the triggering arrangement.

The following results obtained by Gregory and Tinlot (GBP51) clearly illustrate the last point.

In the experiment already discussed in §§ 8.9 and 8.18 these authors operated a multiple-plate cloud chamber so as to select nuclear interactions produced by neutral rays and giving rise to at least one particle capable of traversing a shielded counter telescope placed below the chamber (see Fig. 8.1.18e). They divided the pictures of nuclear events thus obtained into two groups: Group A included events giving rise to one or to two secondary penetrating particles (types 1,2,3,4 in Table 8.9.2).

Group B included events giving rise to 3 or more secondary particles (types 5,6,7,8,9 in Table 8.9.2 and events of similar types with origin above the chamber).

In group A they observed 2 secondary events of ionizing particles in a total thickness of 1,440 g cm^{-2} of lead and 543 g cm^{-2} of aluminum traversed by the secondary particles. In group B they observed 48 secondary events of ionizing particles in a total thickness of 6,017 g cm^{-2} of lead and 2,142 g cm^{-2} of aluminum. In Table 1 the observed secondary events are classified according to the material in which they occur (lead or aluminum) and to the type of interaction (nuclear scattering or more complex interaction). This table also contains data relative to secondary interactions of neutral particles (to be discussed later).

Table 8.19.1. Secondary nuclear interactions recorded by Gregory and Tinlot (GBP51) with the experimental arrangement shown in Fig. 8.1.18e. [x is the total thickness of material traversed by the ionizing secondary particles; n.s. indicates nuclear scattering; n.i. indicates nuclear interaction, exclusive of scattering.]

Primary Event	Secondary Interactions in Lead			
	x (g cm^{-2})	n.i. (ionizing particle)	n.s. (ionizing particle)	n.i. (nonionizing particle)
Group A (low multiplicity)	1440	0	0	3
Group B (high multiplicity)	6017	25	10	6

Primary Event	Secondary Interactions in Aluminum			
	x (g cm^{-2})	n.i. (ionizing particle)	n.s. (ionizing particle)	n.i. (nonionizing particle)
Group A (low multiplicity)	543	2	0	1
Group B (high multiplicity)	2142	10	3	4

One sees that the number of secondary nuclear interactions per unit path length is about six times greater in the second group of pictures than in the first one. The explanation of this difference, of course, lies in the triggering arrangement, which requires the presence of a penetrating particle below the chamber. Most secondary nuclear interactions give

rise only to particles of low energy. Thus a secondary particle that undergoes a nuclear interaction thereby loses, as a rule, its ability to trigger the chamber. This introduces a bias against recording events in which secondary nuclear interactions occur. The magnitude of this bias strongly depends on the number of penetrating particles coming out of the primary interaction. If only one secondary penetrating particle is present and this particle interacts in the chamber, the chamber will usually fail to record the event. If, instead, many secondary penetrating particles are present, the fact that one of them interacts in the chamber will not greatly diminish the probability that the chamber be triggered.

Table 2 lists the mean free path in lead for nuclear interactions of ionizing secondary particles as obtained by several observers with cloud-chamber experiments. The results of Gregory and Tinlot, which seem to be among the most reliable, give a mean free path in lead close to the geometric mean free path (L_g = 164 g cm^{-2}). Since, in all likelihood, a large fraction of the secondary penetrating particles are π-mesons, the above result strongly indicates that the cross-section for the interaction of π-mesons with heavy nuclei is near the geometrical value.

Table 8.19.2. Mean free paths for nuclear interactions of secondary particles in lead as obtained from cloud-chamber observations. [n.s. indicates nuclear scattering; n.i. indicates nuclear interaction other than nuclear scattering. In the computation of the collision mean free path both types of events are considered, unless otherwise stated. The corrections include estimates of the number of events missed and of the bias introduced by the triggering arrangement.]

Author	No. of Secondary Events		L_c (uncorrected) g cm^{-2}	L_c (corrected) g cm^{-2}
	n.i.	n.s.		
Fretter (FWB49.1)	78	12	750	$750 < L < 80$
Lovati (LA50)	29	7	650	600 ± 90
Brown and McKay (BWW50)	30	—	505	316 + 70*
Butler *et al.* (BCC50)	4	3	400 ± 150	—
Gregory and Tinlot (GBP51)	25	10	—	172 ± 30

* Nuclear scattering not considered.

Camerini and his collaborators (CU50) reached a similar conclusion from their work with photographic emulsions. They observed 15 nuclear interactions produced by secondary particles with grain density less than 1.5 minimum (thin tracks). From the total distance traveled by these particles in the emulsion they computed a value of 102 ± 27 g cm^{-2} for the mean free path (the geometric mean free path in the emulsion is about 90 g cm^{-2}). As shown in Table 8.10.1, most of the secondary thin tracks are due to π-mesons, and of the 15 particles considered here 6 were actually identified as π-mesons. The same authors also measured the mean free path for nuclear interactions of secondary particles with medium grain density that could be identified as protons, deuterons, or tritons. For protons they found a value of 120 ± 30 g cm^{-2}, and for deuterons and tritons (considered together) a value of 47 ± 18 g cm^{-2}.

Little experimental information is available as yet on the mean free path of secondary ionizing particles in light elements. The observations of Gregory and Tinlot (see Table 1) give a mean free path in aluminum of 164 ± 50 g cm^{-2}. Since the geometric mean free path in aluminum is 82 g cm^{-2}, there seems to be some indication of transparency of the aluminum nucleus.

Observations on the secondary interactions of neutral particles (neutrons) do not yield information on the mean free path of these particles because their trajectories are not visible and it is thus impossible to refer the number of nuclear interactions to the total amount of material traversed. However, one can use these observations to obtain an estimate for the relative abundance of neutrons and of charged particles among the secondary products of nuclear interactions. Thus, for example, Gregory and Tinlot in their "group B" pictures (see Table 1) found 10 nuclear interactions initiated by secondary neutrons as against 35 nuclear interactions initiated by secondary ionizing particles, while Brown and McKay (BWW50) found a ratio of 1.5 ± 0.4 between the numbers of secondary interactions initiated by charged and neutral particles respectively. (Here, of course, processes of nuclear scattering are disregarded because the nuclear scattering of a neutron cannot be detected.) From these preliminary results, and from the assumption of equal nuclear cross-sections for neutrons and for ionizing particles, one would conclude that the latter are more abundant than the former among the products of nuclear interactions capable of producing further interactions. Since protons and neutrons should occur in approximately equal numbers, the above result is another piece of evidence pointing to the conclusion that some of the charged secondary interacting particles are π-mesons.

8.20. ***Detailed analysis of individual nuclear events.*** In the experimental investigation of high-energy nuclear interactions one can use two different approaches. One can analyze individual events in all possible detail; i.e., try to determine, for each event, the energy of the primary particle as well as the nature, the energy, and the angle of emission of all secondary particles. Or one can make a statistical study of one of the parameters that describe the properties of nuclear interactions, disregarding all other aspects of the interactions. For example, one can

investigate the angle of emission of mesons without considering their energy or the energy of the producing particle, thus disregarding the fact that the angle of emission, the meson energy, and the primary energy are not independent variables.

Presumably only a detailed analysis of nuclear interactions will afford all the information necessary for a complete understanding of these phenomena. However, because of practical difficulties, most of the experimental data available at the time of this writing are of a statistical character.

Among the few attempts at a detailed analysis of individual events we wish to mention here the work of Feld, Lebow, and Osborne (FBT50; OLS50) and that of Lord, Fainberg, and Schein (LJJ50).

Feld and his collaborators carefully examined 14 nuclear events recorded in electron-sensitive emulsions, each involving at least 5 secondary particles of minimum ionization. For the various secondary particles, they determined the direction of emission in space, the grain density, and, in some cases, the mean angle of scattering. In agreement with the results described in § 8.10, they found that the dense tracks include protons, α-particles, and other nuclear fragments, and that most of the medium tracks are protons.

They also found that, if one classifies the stars according to the total charge, Z_d, carried by the dense tracks, one obtains two separate groups. In the first group this charge corresponds to either 3 or 4 electronic charges; in the second group Z_d ranges from 15 to 28 units. It is natural to ascribe the stars of the first group to the light nuclei of the emulsion (C,N,O), and the stars of the second group to the heavy nuclei (Br,Ag). Indeed none of the stars of the second group can correspond to the disintegration of a C, N, or O nucleus. On the other hand, if some of the stars of the first group were due to the disintegration of heavy nuclei one would expect to find also stars with Z_d between 4 and 15.

Notice that the sharp separation found here between stars from light and heavy nuclei is probably related to the fact that the stars were selected from among those containing at least 5 relativistic particles. An interaction giving rise to 5 relativistic particles apparently leaves the nucleus in a highly excited state so that the nucleus emits a large fraction of its charged particles during the ensuing evaporation process.

For each event, Feld and his collaborators computed the average angle of emission, $\langle\theta_\pi\rangle_{\text{av}}$, of the particles responsible for the thin tracks, believed to be mostly π-mesons (see § 8.10). For the light-nuclei interactions they found that the values of $\langle\theta_\pi\rangle_{\text{av}}$ were in agreement with the assumption of multiple meson production; i.e., with the assumption that each meson group was the result of a single collision between the incident nucleon and one of the nucleons of the target nucleus. This conclusion is significant, despite the relative freedom that exists in choosing the angular distribution and the energy of the produced mesons in the center-of-mass system, because, as we have seen in § 8.7, the value of $\langle\theta_\pi\rangle_{\text{av}}$ does not depend critically on this choice.

One may mention that $\langle\theta_\pi\rangle_{\text{av}}$ was found to decrease with increasing multiplicity, a result easily understandable if one considers that the multiplicity of meson production must be an increasing function of the primary energy, and that $\langle\theta_\pi\rangle_{\text{av}}$ is a decreasing function of the same quantity.

For the heavy-nuclei interactions, instead, the experimental value of $\langle\theta_\pi\rangle_{\text{av}}$ was almost always greater than the value predicted for meson production in a single act. This seems to indicate that the meson groups arising from heavy nuclei are partly the result of successive collisions within each nucleus.

Lord, Fainberg, and Schein made a careful analysis of an exceedingly interesting nuclear event, shown in Fig. 8.1.10. As explained in the caption, the event is produced by a particle of minimum grain density, believed to be a high-energy proton. Among the secondary products there are 15 particles of minimum ionization. Of these, 7 are emitted in an extremely narrow cone (0.003 radians half-angle) so that they appear as a single heavy track near the origin of the event. The other 8 relativistic particles are emitted in a cone of about 0.13 radians half-angle. The axes of the narrow cone and of the diffuse cone coincide and are the exact continuation of the trajectory of the incident particle. At a point of the cone marked by the arrow γ in Fig. 8.1.10 two particles originate and travel at a very small angle to one another and to the axis of the cone. In all likelihood, they are two electrons originating from the materialization of a photon. This, in turn, may originate from the decay of a neutral meson or from a process of charge acceleration occurring in the nuclear interaction.

All of the particles of the narrow cone and some of the particles in the diffuse cone remain in the emulsion for more than 10,000 microns. By measuring the distances between neighboring tracks at various points, Lord, Fainberg, and Schein were able to make exceptionally accurate determinations of the Coulomb scattering and thus to determine, for many of the tracks, either the actual value of the product $p\beta$, or a lower limit for this quantity. The results of these determinations are listed in Table 1. One sees that the energies of the particles in the narrow cone are exceedingly large. Indeed the scattering measurements set a lower limit of 1,400 Bev to the combined energy of the secondary ionizing particles. If one considers the likelihood that a number of neutral π-mesons are produced simultaneously with the charged mesons, one concludes that the energy of the primary proton must be at least 3,000 Bev.

Only two nucleons of sub-relativistic velocities are present among the products of the interaction (track B appears to be that of a proton of about 10-Mev energy, and track C corresponds to a proton of 200-Mev energy). This is strong evidence that the observed event is the result of

Table 8.20.1. Analysis of the tracks in the nuclear event shown in Fig. 8.1.10.
[The values of the product $p\beta$ of the momentum times the velocity of each particle are determined by scattering measurements. From Lord, Fainberg, and Schein (LJJ50).]

Track (numbered from right to left in Fig. 8.1.10).	Length of Track in Emulsion (microns)	$p\beta$ (Bev/c)
B	176	0.01
C	2,700	0.36
Electron pair 1	3,450	3.6
Electron pair 2	4,200	3.0
Diffuse cone		
1	605	—
2	1,300	—
3	10,600	—
4	3,040	—
5	9,630	3.91
6	2,310	2.6
7	2,360	—
8	2,620	—
Narrow cone		
1′	6,990	50
2′	9,400	>250
3′	10,250	>250
4′	11,700	>250
5′	11,700	>250
6′	10,000	>250
7′	9,500	86

a single collision between the incident proton and a nucleon of the target nucleus. Therefore we are dealing here, in all likelihood, with an example of multiple meson production.*

Since the number of mesons is fairly large one may assume that the symmetry principle approximately applies to the event under consideration (even though, strictly speaking, this principle describes only an average property of nuclear events). We thus conclude that approximately equal numbers of mesons are emitted in the forward and in the backward directions in the frame of reference in which the center of mass of the two colliding nucleons is at rest. It is then natural to regard the particles of the narrow cone as the mesons emitted in the forward direction in the center-of-mass system, and the particles of the diffuse cone as the mesons emitted in the backward direction in the center-of-mass system. This

* Note that there is no direct evidence that all of the relativistic particles are π-mesons. Indeed, according to some theoretical views (FE50), one might expect that some of them are protons and anti-protons produced as pairs in the interaction.

view is confirmed by the fact that the particles of the diffuse cone appear to have considerably smaller momenta than the particles of the narrow cone.

The sharp separation between the two cones in the laboratory system suggests that the mesons are not emitted with spherical symmetry in the center-of-mass system, but are rather confined to two opposite cones (see Fig. 1). If θ_1^* is the half-angle of each cone in the center-of-mass system, and if the mesons are emitted in the center-of-mass system with

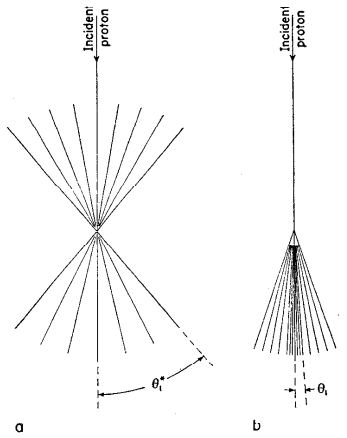

Fig. 8.20.1. Schematic representation of the interaction shown Fig. 8.1.10. (a) The interaction in the center of mass system; (b) the interaction in the laboratory system.

velocity practically equal to the light velocity, the half-angle of the narrow cone in the laboratory system is given by the equation:

$$\tan \theta_1 = \sqrt{\frac{2Mc^2}{U}} \tan\left(\frac{\theta_1^*}{2}\right), \tag{1}$$

where U is the energy of the incident proton [see Eqs. (8.7.5) and (8.7.6)].

Lord, Fainberg, and Schein assumed for θ_1^* a value of 40° and thus obtained, from Eq. (1) and from the measured value of θ_1, $U = 3 \cdot 10^4$ Bev. On the other hand, if one assumes that U is close to the minimum value of $3 \cdot 10^3$ Bev determined above, Eq. (1) yields a value of about 13° for the half-angle of the meson cone in the center-of-mass system.

8.21. ***Nuclear interactions of μ-mesons.*** In § 8.4 we noted that the rate of occurrence of nuclear interactions some distance below ground is exceedingly small. However, already in 1939, Braddick and Hensby

(BJJ39) reported some cloud-chamber observations indicating that nuclear interactions could still be detected at a depth of 6,000 g cm^{-2} underground. George and Trent (GEP49.1) working with a penetrating-shower detector, tentatively reached the same conclusion, although measurements with a somewhat different experimental arrangement had failed to discover any nuclear effect at a similar depth (GEP47).

More definite information on this question came from a preliminary report of some work by George and Evans (GEP50.1). As detectors of nuclear interactions these authors used photographic emulsions prepared at a depth of 6,000 g cm^{-2} at the Holborn Station of the London underground trains. The purpose, of course, was to avoid the production of stars by the N-radiation present aboveground during the time interval between the preparation of the plates and their storage underground.

George and Evans used two different types of emulsions; i.e., the electron-insensitive Ilford C2 emulsion and the electron-sensitive Ilford G5 emulsion. The Ilford C2 plates were left at 6,000 g cm^{-2}, whereas the Ilford G5 plates were stored partly at 6,000 g cm^{-2}, partly at 3,400 g cm^{-2}, and partly at 2,000 g cm^{-2}. Inspection of the plates after an exposure of several months revealed a small but definite production of stars at all depths underground. Table 1 shows the rate of production of stars at the various depths and, for comparison, the rate of production at sea level.

Table 8.21.1. Rate of production of stars at sea level and at various depths underground [from George and Evans (GEP50.1)].

Depth Below Sea Level (g cm^{-2})	Number of Stars Observed	Number of Stars (per cm^3 day)
0	383	1.46 ± 0.07
2000	7	0.0066 ± 0.0025
3400	13	0.0044 ± 0.0012
6000	22	0.0050 ± 0.0010

Altogether 42 nuclear interactions giving rise to stars with three or more prongs were recorded underground. Of these, 24 occurred in Ilford G5 emulsions and 18 in Ilford C2 emulsions. Among the 24 stars occurring in Ilford G5 emulsions, 10 appeared to be initiated by ionizing particles of minimum grain density, 14 by non-ionizing particles. The 14 stars initiated by non-ionizing particles contained only dense and medium tracks. Of the 10 stars initiated by ionizing particles, 5 stars had one secondary thin track and 4 stars had two or more thin secondaries. Since the Ilford C2 emulsions do not record thin tracks, no similar classification could be made for the stars occurring in these emulsions.

Table 1 shows that as one goes from sea level to greater and greater depths underground, the rate of occurrence of nuclear interactions decreases very rapidly at first but then becomes almost stationary. As already pointed out in § 8.5, the initial fast decrease indicates that most of the events observed at sea level are due to particles with large cross-sections for nuclear collisions; i.e., to neutrons, protons, and perhaps π-mesons. However, the subsequent slow decrease of the star rate proves that cosmic-ray particles much more penetrating than those just mentioned also are capable of producing nuclear disintegrations. Mu-mesons are the only known particles whose penetrating power is sufficiently great to explain the small change of star production between 2,000 and 6,000 g cm^{-2}. There is thus little doubt that μ-mesons are responsible, directly or indirectly, for practically all of the nuclear interactions observed at depths greater than about 2,000 g cm^{-2} underground.

It is likely that μ-mesons produce directly those stars that appear to be initiated by ionizing particles. From the rate of occurrence of such stars at 6,000 g cm^{-2} depth and from the known flux of μ-mesons at this depth, George and Evans concluded that μ-mesons have a cross-section for nuclear interactions of the order of 10^{-29} cm^2 per nucleon, or a collision mean free path of the order of $2 \cdot 10^5$ g cm^{-2}.

As mentioned above, many of the stars that we consider to be initiated by μ-mesons contain the track of one secondary fast particle. This track usually forms a small angle with the track of the incident μ-meson. George and Evans suggested that stars of this kind are the result of a simple scattering process of a μ-meson by a nucleon of the target nucleus. In this process the recoil nucleon acquires enough energy to produce a nuclear evaporation, whereas the scattered meson itself gives rise to the observed thin star track. The same authors suggested also that the stars containing groups of secondary fast particles may be examples of π-meson production by μ-mesons. They indicated that this process may be explained as an electromagnetic effect. In fact, it is possible to describe the electric field of a charged particle with relativistic velocity as a flux of photons (WC34). As discussed in § 7.12, photons of sufficiently high energy interact with nucleons to produce π-mesons.

Nuclear interactions of μ-mesons with nucleons certainly give rise, among other particles, to neutrons in the 100-Mev energy range. It is likely that these neutrons are responsible for most of the underground stars that appear to be initiated by neutral particles. Some of these stars, however, may be produced by photons, which are known to exist underground and which arise from electromagnetic interactions of μ-mesons.

It is interesting to notice that none of the 14 underground stars initiated by neutral particles contain secondary fast particles. This observation agrees with the assumption that the stars in question are produced by secondary neutrons and photons of comparatively low energies.

8.22. ***Nuclear interactions of complex nuclei.*** Balloon observations by the cosmic-ray groups at Rochester and Minnesota (FP48.1; FP48.2; BHL48; BHL50.1; BHL50.4) have shown that α-particles and heavier nuclei of great energies exist in appreciable numbers at high altitudes. These multiply charged nuclei have been recorded both with cloud chambers and with photographic emulsions, but their properties have been studied mainly with the latter method.

In photographic emulsions, α-particles can be identified from the grain density (which, at relativistic velocities is four times $g_{\min}$). Nuclei with more than five units of charge can be identified from the δ-ray density. Recently Bradt and Peters (BHL50.4) have succeeded in identifying nuclei with charges 3, 4, or 5 by grain counting in under-developed emulsions.

There is strong evidence that these multiply charged nuclei are part of the primary radiation (according to Bradt and Peters, however, nuclei with 3, 4, or 5 units of charge do not belong to the primary radiation but arise from the disintegration of heavier nuclei in the atmosphere above the plates). Table 1, compiled from the data of Bradt and Peters (BHL50.1; BHL50.4), gives the estimated flux of protons and of various groups of

Table 8.22.1. Flux of protons and of heavier nuclei in the primary cosmic radiation at 30° N geomagnetic latitude. [From Bradt and Peters (BHL50.1; BHL50.4).]

Element	Z	Nuclei per m^2-sec-sterad	Per cent of Sum of Nuclei	Nucleons per m^2-sec-sterad	Per cent of Sum of Nucleons
H	1	356	79.0	356	45.0
Li, Be, B	3,4,5	none detected			
He	2	90	20.0	360	45.3*
C, N, O	6,7,8	3.5	.78	49	6.2
	$Z > 10$	1	.22	28	3.5
Sum of above:		450.5	100	783	100

* According to a private communication from B. Peters to the author (February 1951) later measurements make it appear likely that the α-particle flux is about 30 per cent less than the value given in this table.

heavier nuclei incident upon the top of the atmosphere at 30° N geomagnetic latitude. The presence of complex nuclei in the primary cosmic radiation is a matter of great importance in connection with the problem of the origin of cosmic rays and with the general interpretation of cosmic-ray phenomena. Here, however, we shall concern ourselves only with the observations on the heavy primaries in so far as they yield information on the nuclear interactions of complex nuclei of very great energies.

Several authors have published pictures of such interactions obtained with the method of the photographic emulsion. Examples are shown in Figs. 8.1.12, 8.1.13, 8.1.14, and 8.1.15. The photographic plates are usually exposed in stacks. Since the tracks of multiply charged nuclei have a very characteristic appearance, it is comparatively easy to follow them through a number of plates. Bradt and Peters (BHL50.1; BHL50.4) have taken advantage of this circumstance to determine the collision mean free paths in glass (supporting the emulsion) for three groups of multiply charged nuclei. The results obtained are summarized in Table 2. Hoang-Tchang-Fong (HTF50), instead, has determined the mean free paths in the photographic emulsion itself for two groups of multiply charged nuclei by dividing the total length of track observed by the number of nuclear interactions occurring in the emulsion. The results are shown in Table 3.

If one represents both the incident nucleus (atomic mass number A) and the target nucleus (atomic mass number A') as spheres of radii $r_n = r_0 A^{1/3}$ and $r'_n = r_0(A')^{1/3}$ respectively, one obtains for the geometric collision cross-section the value:

$$\sigma_g = \pi r_0^2 [A^{1/3} + (A')^{1/3}]^2. \tag{1}$$

Table 8.22.2. Mean free path for nuclear collisions of high-energy nuclei in glass. [As measured by Bradt and Peters (BHL50.4) and as computed on the basis of the cross-sections given by Eq. (1). (The observed nuclei with Z between 3 and 5 probably did not belong to the primary radiation but were produced in the air above the plates by nuclear collisions of heavier nuclei.)]

Z of Incident Nucleus	Number of Collisions Observed	Mean Free Path in g cm^{-2}	
		Observed	Computed from Eq. (1)
3–5	5	47	25
6–8	59	34 ± 4	22
10–18	36	26 ± 4	18
19–26	11	23 ± 7	13

Table 8.22.3. Mean free path for nuclear collisions of high-energy nuclei in photographic emulsion. [As measured by Hoang-Tchang-Fong (HTF50) and as computed from the cross-sections given by Eq. (1).]

Z of Incident Nuclei	Mean Free Path in g cm^{-2}	
	Observed	Computed, Eq. (1)
$3 < Z < 10$	37	28
$Z \geq 10$	25	17

Tables 2 and 3 list the mean free paths corresponding to the geometric cross-sections given by Eq. (1). One sees that the mean free paths thus computed are in all cases shorter than the observed mean free paths. Bradt and Peters have tentatively interpreted this result by assuming that an interaction occurs only when there is a certain amount of overlapping between the spheres that represent the two colliding nuclei.

We shall now examine briefly the phenomena that take place when two complex nuclei collide.

In many cases one can interpret the observed event by assuming that the two nuclei traverse one another without any too violent nucleon-nucleon collision. As a consequence of this interaction, both nuclei may acquire excitation energies of the order of several hundred Mev. Subsequently the two nuclei disintegrate, each giving rise to a "star" of comparatively slow nuclear fragments in its own frame of reference. The disintegration products of the target nucleus appear in the photographic emulsion as an ordinary low-energy star with mainly dense tracks, which are distributed randomly in direction. The disintegration products of the incident nucleus, instead, appear as a group of particles moving with approximately the initial velocity of the incident nucleus itself, and concentrated in a cone whose aperture is smaller the greater the velocity of the incident nucleus.

Figure 8.1.12, reproduced from a paper by Bradt and Peters (BHL50.1), offers a particularly clear example of the process just described. In this case the narrow cone consists of five α-particles and a proton arising from the disintegration of the incident nucleus. No meson tracks are visible.

Hoang-Tchang-Fong (HTF50) has analyzed in detail a case in which the incident nucleus appears to disintegrate into seven protons (plus, presumably, an approximately equal number of undetectable neutrons). Again there is no evidence of meson production. From the grain density of the proton tracks one can estimate the proton energies. After making allowance for the energy that goes into the neutrons, one obtains a value between 6 and 7 Bev for the kinetic energy of the incident nucleus. Since the atomic mass number of this nucleus is close to 14, the kinetic energy per nucleon is 0.5 Bev or somewhat less. At this energy the cross-section for meson production is small compared with the total collision cross-section, and it is therefore not astonishing that mesons do not appear among the secondary products of the interaction.

Figure 8.1.13, from a paper by Leprince-Ringuet and his collaborators (LRL49.2; LRL49.3), shows a very impressive example of a process of the same general type. It represents the complete disintegration of a target silver nucleus ($Z = 47$) and of an incident nucleus with Z close to 18. The total energy released is about 14 Bev and there is no evidence that any of the secondary particles are mesons, even though the existence of a few meson tracks cannot be ruled out.

In the cases considered so far the energy per nucleon of the incident nucleus is not very large, even though the kinetic energy of the nucleus as a whole may be of the order of 10^{10} ev. Several experimenters have reported observing the nuclear interaction of a multiply charged nucleus whose energy per nucleon was large compared with one Bev. As one might have expected, mesons figure prominently among the secondary products of these interactions.

Bradt, Kaplon, and Peters (BHL50.3, KMF49), in a survey of electron-sensitive plates (Kodak NTB3) flown at an altitude of 30,000 meters, observed an exceedingly interesting event of this kind (see Fig. 8.1.15). The event is produced by an α-particle of relativistic velocity. It gives rise to 18 particles of subrelativistic velocities (protons and heavier nuclear fragments), to one α-particle of about 2.5-Bev energy, and to about 55 singly charged particles of approximately minimum ionization. The 18 subrelativistic particles arise clearly from the explosion of the target nucleus. They carry at least 23 units of charge and an energy of approximately 2.8 Bev. The heaviest nucleus in the emulsion is silver ($Z = 47$) and the incident α-particle has 2 units of charge. Of the 49 units of charge present in the colliding nuclei, at least 23 are accounted for by the subrelativistic disintegration products and 2 by the fast secondary α-particle. One thus concludes that of the 55 relativistic singly charged particles at most 24 are protons. It is very likely that the remaining 31 are π-mesons, and the number of π-mesons may be even greater.

The 55 relativistic particles fall into two distinct groups. About 23 of them are contained in a very narrow cone whose axis is an exact continuation of the trajectory of the incident α-particle. The remaining 32 particles have a wide angular distribution. Figure 1 gives the angular distribution of all 55 relativistic particles. There is definite evidence that the narrow cone, in addition to the 23 ionizing particles believed to be π-mesons, also contains many high-energy photons. In fact, after

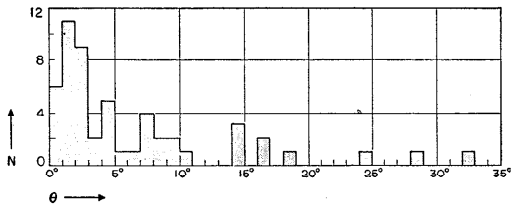

Fig. 8.22.1. Angular distribution with respect to the incident α-particle, of the 55 relativistic particles arising from the nuclear interaction shown in Fig. 8.1.15. The abscissa represents the projected angle in the plane of the emulsion. [From Bradt *et al.* (BHL50.3).]

passing through 2 cm of glass into the emulsion of the next plate of the stack, the cone appears to contain 44 relativistic particles instead of the original 23. The additional particles are believed to be electrons produced (mostly in the glass) by materialization of photons. This assumption is confirmed by the direct observation of two electron pairs produced in the emulsion, within the narrow cone. From the separation between the two electrons of each pair one can compute the energy of the corresponding photon. This energy is of the order of 50 Bev for the first pair and 10 Bev for the second. The high-energy photons present in the narrow cone probably arise from the decay of neutral mesons.* Bradt, Kaplon, and Peters estimated the average energy of these neutral mesons to be approximately 18 Bev. If one assumes that the charged mesons in the narrow cone have the same average energy as the neutral mesons and that the number of neutral mesons is one-half that of the charged mesons, one obtains a value of $18 \cdot 23 \cdot 1.5 \approx 600$ Bev for the total energy of the mesons in the narrow cone alone. Thus the energy of the primary α-particle cannot have been smaller than about 10^{12} ev.

Probably the mesons belonging to the narrow cone have been produced directly in the collisions of the four nucleons of the incident α-particle with an equal number of nucleons of the target nucleus. The average multiplicity of charged and neutral mesons in the individual nucleon-nucleon collisions would thus be of the order of 9. Bradt, Kaplon, and Peters have discussed in detail this assumption in relation to the observed angular distribution. They have come to the conclusion that if the angular distribution of the mesons is approximately isotropic in the center-of-mass system of each pair of colliding nucleons, one must assign to the incident α-particle an energy of the order of 10^{13} ev in order to explain the small angle of emission of the mesons in the laboratory system. In this case the energy going into mesons in the center-of-mass system is only a small fraction of the available energy. If, on the other hand, one assumes that most of the available energy goes into mesons, the energy of the incident α-particle is of the order of 10^{12} ev and the observed angular distribution can be explained only if the emission of mesons in the center-of-mass system is strongly anisotropic.

Of the 32 relativistic particles emitted at wide angles some are mesons, some probably protons. If one assumes strong anisotropy for meson production in the center-of-mass system, it becomes possible to explain both the narrow cone and the diffuse shower of mesons as being simultaneously produced in the primary encounters. Under this assumption, the narrow cone corresponds to the group of mesons emitted in the forward direction in the center-of-mass system, the diffuse shower corresponds to

* Incidentally, from the fact that γ-rays are present so close to the point where the interaction occurs, one obtains an upper limit of about $3 \cdot 10^{-13}$ sec for the mean life of neutral mesons (see § 4.15).

the group of mesons emitted in the backward direction. Indeed, the symmetry principle requires that both groups should be present.

If, however, one assumes approximately isotropic emission of mesons in the center-of-mass system (and consequent higher energy for the primary α-particle) all of the mesons produced in the primary collisions are emitted, in the laboratory system, within a single narrow cone. In this case, the diffuse group must be due to subsequent collisions of the particles produced in the primary encounter.

Another interesting case of meson production by the nuclear collision of a heavy nucleus has been described by Freier and Ney (FP50).

In a survey of electron-sensitive emulsions exposed at balloon altitudes these authors observed a multiply charged nucleus, probably a carbon nucleus, interact in the emulsion, losing not more than one unit of charge and continuing its trajectory without being appreciably deflected. The interaction gives rise to 11 minimum-ionizing particles in a narrow cone, and to one slow proton at 102° from the direction of the incoming particle. The event is interpreted as follows. The incident carbon nucleus, of about 60 Bev energy per nucleon, encounters a hydrogen nucleus in the emulsion. One of the protons of the carbon nucleus collides with the proton at rest. The collision gives rise to 10 charged mesons, which account for 10 of the 11 thin tracks in the narrow cone. After the collision, the two protons rebound 180° apart in the center-of-mass system. The proton that is projected backward in the center-of-mass system appears in the laboratory system as a 5-Mev proton at 102°. The proton projected forward gives rise to the eleventh thin track of the narrow cone.